Mon. Not. R. Astron. Soc. **000**, 000–000 (0000) Printed 1 February 2010 (MN LATEX style file v2.2)

Chasing the heaviest black holes of jetted Active Galactic Nuclei

G. Ghisellini[1⋆], R. Della Ceca[2], M. Volonteri[3], G. Ghirlanda[1], F. Tavecchio[1], L. Foschini[1], G. Tagliaferri[1], F. Haardt[4,5], G. Pareschi[1], J. Grindlay[6]

[1]*INAF – Osservatorio Astronomico di Brera, Via Bianchi 46, I–23807 Merate, Italy*
[2]*INAF – Osservatorio Astronomico di Brera, Via Brera 28, I–20100 Milano, Italy*
[3]*Astronomy Department, University of Michigan, Ann Arbor, MI 48109*
[4]*Universitá dell'Insubria, Dipartimento di Fisica e Matematica, Via Valleggio 11, I–22100 Como, Italy;*
[5] *INFN, Sezione di Milano-Bicocca, I–20126 Milano, Italy*
[6]*Harvard–Smithsonian CfA, 60 Garden Street Cambridge MA 02138, USA*

arXiv:0912.0001v2 [astro-ph.HE] 1 Feb 2010

1 February 2010

ABSTRACT

We investigate the physical properties of the 10 blazars at redshift greater than 2 detected in the 3–years all sky survey performed by the Burst Alert Telescope (BAT) onboard the *Swift* satellite. We find that the jets of these blazars are among the most powerful known. Furthermore, the mass of their central black hole, inferred from the optical–UV bump, exceeds a few billions of solar masses, with accretion luminosities being a large fraction of the Eddington one. We compare their properties with those of the brightest blazars of the 3–months survey performed by the Large Area Telescope (LAT) onboard the *Fermi* satellite. We find that the BAT blazars have more powerful jets, more luminous accretion disks and larger black hole masses than LAT blazars. These findings can be simply understood on the basis of the blazar sequence, that suggests that the most powerful blazars have a spectral energy distribution with a high energy peak at MeV (or even sub–MeV) energies. This implies that the most extreme blazars can be found more efficiently in hard X–rays, rather than in the high energy γ–ray band. We then discuss the implications of our findings for future missions, such as the *New Hard X–ray Mission (NHXM)* and especially the *Energetic X–ray Imaging Survey Telescope (EXIST)* mission which, during its planned 2 years all sky survey, is expected to detect thousands of blazars, with a few of them at $z \gtrsim 6$.

Key words: BL Lacertae objects: general — quasars: general — radiation mechanisms: non–thermal — gamma-rays: theory — X-rays: general

1 INTRODUCTION

Ajello et al. (2009, hereafter A09) recently published the list of blazars detected in the all sky survey by the Burst Alert Telescope (BAT) onboard the *Swift* satellite, between March 2005 and March 2008. BAT is a coded mask designed to detect Gamma Ray Bursts (GRBs), has a large field of view ($120^\circ \times 90^\circ$, partially coded) and is sensitive in the [15–150 keV] energy range. This instrument was specifically designed to detect GRBs, but since GRBs are distributed isotropically in the sky, BAT, as a by–product, performed an all sky survey with a reasonably uniform sky coverage, at a limiting sensitivity of the order of 1 mCrab in the 15–55 keV range (equivalent to 1.27×10^{-11} erg cm^{-2} s^{-1}) in 1 Ms exposure (A09). Taking the period March 2005 – March 2008, and evaluating the image resulting from the superposition of all observations in this period, BAT detected 38 blazars (A09), of which 26 are Flat Spectrum Radio Quasars (FSRQs) ad 12 are BL Lac objects, once the Galactic plane ($|b < 15^\circ|$) is excluded from the analysis. A09 reported an average exposure of 4.3 Ms, and considered the [15–55 keV] energy range, to avoid background problems at higher energies. The well defined sky coverage and sources selection criteria makes the list of the found blazars a complete, flux limited, sample, that enabled A09 to calculate the luminosity function and the possible cosmic evolutions of FSRQs and BL Lacs, together with their contribution to the hard X–ray background. A09 also stressed the fact that the detected BAT blazars at high redshift are among the most powerful blazars and could be associated with powerful accreting systems.

Within the BAT sample, there are 10 blazars (all FSRQs) at redshift greater than 2, and 5 at redshift between 3 and 4. For comparison, the Large Area Telescope (LAT) onboard the *Fermi* satellite detected about one hundred blazars (at high significance in the first 3 months), with a maximum redshift of 2.944 (Abdo et al. 2009). Only 5 blazars have $z > 2$, with only 1 with $z > 2.5$.

⋆ Email: gabriele.ghisellini@brera.inaf.it

© 0000 RAS

Fig. 1 shows the distribution of redshifts for the *Fermi*/LAT and the *Swift*/BAT blazars. Comparing the two redshift distributions and including BL Lac objects, a K–S test gives a probability $P = 0.079$ that they are drawn from the same distribution, that decreases to $P = 0.034$ when excluding BL Lacs. The BAT FSRQs have a tail at high redshifts, not present in the case of LAT FSRQs. This presence of this tail in the redshift distribution of BAT blazars is the first indication that a survey in hard X–rays can be more fruitful in pinpointing the most powerful blazars lying at the highest redshifts. Theoretically, this can be understood on the basis of the blazar sequence (Fossati et al. 1998; Ghisellini et al. 1998, Donato et al. 2001; Ghisellini, Maraschi & Tavecchio 2009). According to this sequence the most powerful blazars, that are all FSRQs, have the high energy peak of their spectral energy distribution (SED) in the MeV range. As a consequence, these objects are more luminous in hard X–rays than what they are above 100 MeV, and thus become detectable in the BAT survey even if they are undetected in the LAT one. Indeed, *none* of the 10 BAT blazars at $z > 2$ is present in the 3–months LAT survey of bright blazars, while 4 are present in the *Fermi*/LAT 11 months survey catalogue of sources with a $> 4\sigma$ level detection[1] (PKS 0537–286, 0746+254, 0805+6144 and 0836+710), and one additional source (PKS 2149–306) has a *Fermi*/LAT detection reported by Böck et al. (2010). The *Fermi*/LAT fluxes of these sources are just above the limiting sensitivity for a 5σ detection in 1 yr survey.

The aim of the present paper is to study the most powerful and distant blazars present in the BAT survey in order to estimate the power carried by their jets in the form of bulk motion of matter and fields. Furthermore, we will estimate the mass of their central black hole and their accretion disk luminosities. To this aim we will take advantage of the data of the other *Swift* instruments (the X–ray Telescope, XRT, and the UV and Optical Telescope, UVOT). We will then compare the overall properties of these powerful BAT blazars with the same properties of the bright γ–ray blazars detected by the LAT and recently studied in Ghisellini et al. (2010, hereafter G10).

Finally, we will discuss the implications of our findings for the future missions, such as *NHXM* and *EXIST*, highlightening the possible discovery space that these missions can have concerning the search and the study of the largest black hole masses of jetted sources at large redshift.

We use a flat cosmology with $h_0 = \Omega_\Lambda = 0.7$. We adopt the convention $Q = 10^x Q_x$ and use cgs units unless specified otherwise.

2 THE SAMPLE

In A09 all BAT blazars were fitted with a simple power law in the 15–55 keV energy range. The resulting energy spectral indices α_X are shown in Fig. 2 as a function of the rest frame [15–55 keV] luminosity, calculated according to:

$$L_X = 4\pi d_{\rm L}^2 \frac{F_X}{(1+z)^{1-\alpha_X}} \qquad (1)$$

where F_X is the observed X–ray flux in the 15–55 keV energy range as listed in A09.

Blazars with $z > 2$ are marked with black diamonds: they are the most luminous, with $L_X > 2\times 10^{47}$ erg s^{-1} in the (rest frame) 15–55 keV band. Our cut in redshift therefore corresponds also to a cut in luminosity, as expected for a flux limited sample.

[1] http://fermi.gsfc.nasa.gov/ssc/data/access/lat/1yr_catalog/

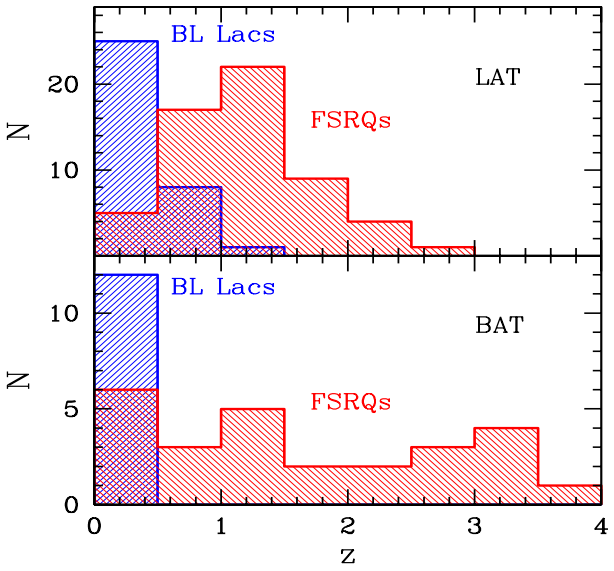

Figure 1. Comparison of the redshift distributions of the bright *Fermi*/LAT and *Swift*/BAT blazars, divided in BL Lacs and FSRQs.

Name	Alias	z	F_X	α_X	$\log L_X$
0014+813	S5	3.366	1.88±0.21	0.93±0.55	48.03
0222+185	RBS315	2.69	1.42±0.22	0.48±0.45	47.63
0537–286	PKS	3.10	1.27±0.20	0.56±0.30	47.75
074625+2549	SDSS	2.98	1.49±0.25	0.08±0.38	47.50
0805+6144	GB6	3.033	0.96±0.19	0.58±0.62	47.62
0836+710	4C71.07	2.17	2.85±0.18	0.47±0.14	47.73
1210+330	B2	2.50	0.90±0.17	0.40±0.30	47.32
2126–158	PKS	3.268	1.55±0.27	0.72±0.68	47.99
2149–306	PKS	2.35	3.72±0.26	0.52±0.21	47.95
225155+2217	MG3	3.668	1.00±0.19	0.51±0.33	47.77

Table 1. The 10 BAT blazars in A09 with $z > 2$. The flux F_X is in units of 10^{-11} erg cm^{-2} s^{-1} and is calculated in the 15–55 keV energy range. The luminosity L_X is calculated according to Eq. 1 and is in units of erg s^{-1}.

Table 1 reports the redshift, the BAT X–ray flux in the 15–55 keV range, the energy spectral index in this energy range and the corresponding K–corrected X–ray luminosity. Is should be noted that these 10 blazars *are not* the only $z > 2$ blazars detected by BAT. Indeed, there are 4 additional blazars in the $|b| < 15^\circ$ region (0212+735, with $z = 2.367$; OA 198 at $z = 2.365$; SWIFT J1656.3–3302 at $z = 2.4$ and PKS 1830–211 at $z = 2.507$), which are present in the catalogues of Cusumano et al. (2009) and of Tueller et al. (2009) We chose the A09 catalogue mainly because of their derivation of the blazar luminosity function performed with the data in that paper.

Several of the sources listed in Tab. 1 have already been discussed and modelled in the literature: S5 0014+813 was discussed by Ghisellini et al. (2009) because of its apparently huge black hole mass (40 billion solar masses, but see Ghisellini et al. 2009 for the possibility that this is over–estimated because of the assumption of an isotropically emitting accretion disk, and see below for further

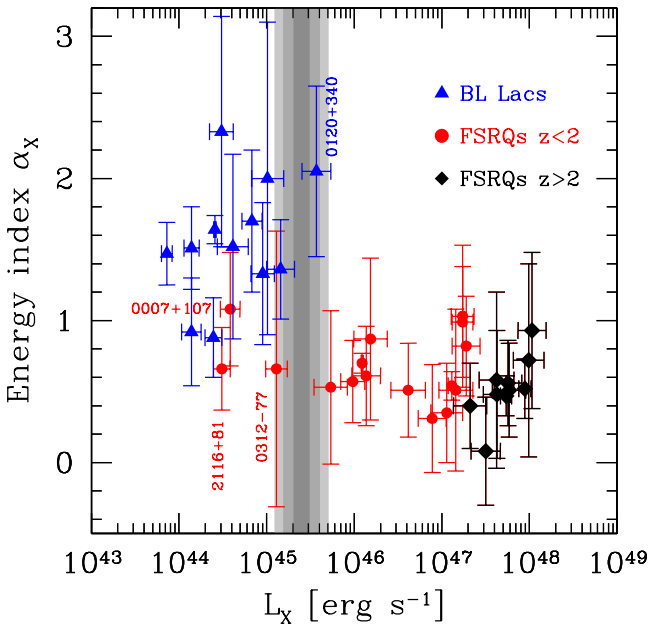

Figure 2. The X–ray energy spectral index α_X as a function of the luminosity in the BAT energy range 15–55 keV. In this plane BL Lacs (triangles) and FSRQs (circles and diamonds) are clearly separated. We also mark (black diamonds) the FSRQs with $z > 2$. The labelled sources are the BL Lac 1ES 0120+340 ($z = 0.272$) and the three sources classified as FSRQs by A09 to the left of the divide. Note that of these three objects, B0007+107 (= Mkn 1501) is a Seyfert 1 galaxy at $z = 0.09$ with a superluminal jet (Brunthaler et al. 2000) and S5 2116+81 ($z = 0.084$) is a radio–galaxy (Stickel, Kühr & Fried 1993). The grey stripes indicate the X–ray luminosity dividing BL Lacs from FSRQs.

discussion); RBS 315 was discussed in Tavecchio et al. (2007, presenting also Suzaku data), PKS 0537–286 is discussed in Sambruna et al. (2007) and in Bottacini et al. (2010, presenting also *INTEGRAL* data); J074625+2549 is discussed in Sambruna et al. (2006) and Watanabe et al. (2009, presenting also *Suzaku* data); 4C 71.07 (=0836+710) is discussed in Foschini et al. (2006) and Sambruna et al. (2007); PKS 2149–306 is discussed in Sambruna et al. (2007) and in Bianchin et al. (2009, presenting also XMM–*Newton* and *INTEGRAL* data); J225155+2217 is discussed in Bassani et al. (2007, presenting also *INTEGRAL* data), and in Maraschi et al. (2008).

To the best of our knowledge, the overall SED of the remaining 3 blazars: GB6 J0805+6144, B2 1210+330 and PKS 2126–158 have not yet been discussed and modelled.

2.1 The BAT blazars' divide

Fig. 2 shows that BL Lacs and FSRQs are clearly separated in the α_X–L_X plane: BL Lacs have steeper slopes and lower luminosities than FSRQs. This can be readily explained recalling that, in BL Lacs, the X–ray flux often belongs to the tail of the synchrotron hump, while in more powerful FSRQs the X–ray flux always belongs to the very hard portion of the high energy hump, believed to be produced by Inverse Compton process. The separation occurs at $\alpha_X \sim 1$ and at $L_X \sim 10^{45}$ erg s^{-1}. This "divide" is related to a similar divide present in the $\alpha_\gamma - L_\gamma$ plane (Ghisellini, Maraschi & Tavecchio 2009), using the 3–months data of the Fermi/LAT survey. However, there is one important difference: in the $\alpha_\gamma - L_\gamma$ plane BL Lacs are the *hard* sources, while FSRQs are the softer ones. In the γ–ray energy range the flux originates from the same (Inverse Compton) component, and low luminosity BL Lacs peaks at energies close to the end of the LAT energy range, or even at higher energies, and therefore have γ–ray slopes flatter than FSRQs, which instead peaks at energies smaller than 100 MeV. Fig. 2 is therefore another manifestation of the blazar sequence, because it agrees with the ideas that low power blazars have both the synchrotron and the Compton peaks at larger frequencies than FSRQs. In this sense we have "blue" BL Lacs and "red" FSRQs. We propose here that the existence of a dividing X–ray luminosity is the same as discussed in Ghisellini, Maraschi & Tavecchio (2009), namely a change in the accretion regime of the underlying accretion disk. This interpretation assumes that there is a connection between the non–thermal beamed luminosity and the thermal luminosity produced by accretion, and that the range of black hole masses of the blazars illustrated in Fig. 2 is relatively small. Within this context, the most luminous objects are the ones accreting close to the Eddington rate. The dividing X–ray luminosity is produced by objects whose accretion disk is accreting at a rate a factor ~ 300 lower. If these sources have the same mass as the most powerful blazars, then they accrete at the 0.3% of the Eddington rate, and at these rates the accretion could change regime, becoming radiatively inefficient (see the discussion in Ghisellini, Maraschi & Tavecchio 2009). In turn, the rather abrupt decrease of ionising photons occurring at and below the critical accretion rate implies an equally abrupt decrease of the broad line luminosity, making the blazar appear as a line–less BL Lac.

3 SWIFT DATA AND ANALYSIS

We collected the public *Swift* data of the 10 sources listed in Tab. 1. For all but one source, B2 1210+330, we could find at least one observation in the Swift archive. We obtained a *Swift* ToO for this source: the observations were performed on the 26th and 27th of October 2009.

3.1 XRT data

The XRT data were processed with the standard procedures (`XRTPIPELINE v.0.12.2`). We considered photon counting (PC) mode data with the standard 0–12 grade selection. Source events were extracted in a circular region of aperture $\sim 47''$, the background was estimated in a same sized circular region far from the source. Response matrices were created through the `xrtmkarf` task. The channels with energies below 0.3 keV and above 10 keV were excluded from the fit and the spectra were rebinned in energy so to have at least 30 counts per bin. For spectra with very few counts, the Cash statistics was applied. When a sufficiently long exposure is available, we present the data corresponding to that observations. In a few cases we summed the data of different observations, to have a more accurate fit, after having checked that the fits of the single observations gave consistent results.

Each spectrum was analysed through XSPEC with an absorbed power–law using the Galactic column density ($N_{\rm H}^{\rm Gal}$ from Kalberla et al. 2005). The computed errors represent the 90% confidence interval on the spectral parameters. In Table 2 we list the results.

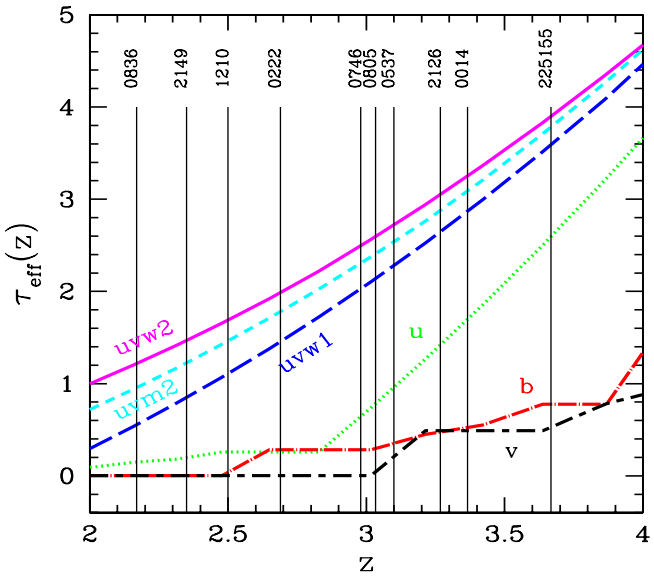

Figure 3. The optical depth due to neutral hydrogen and helium as a function of redshifts. Vertical lines (and labels) indicate the redshifts of the blazar in our sample. The different curves are for the 6 filters of UVOT, as labelled.

3.2 UVOT data

UVOT (Roming et al. 2005) source counts were extracted from a circular region $5''-$sized centred on the source position, while the background was extracted from a larger circular nearby source–free region. Data were integrated with the `uvotimsum` task and then analysed by using the `uvotsource` task.

The observed magnitudes have been dereddened according to the formulae by Cardelli et al. (1989) and converted into fluxes by using standard formulae and zero points from Poole et al. (2008). No further absorption was applied. Tab. 3 lists the result.

4 LYMAN–α AND LYMAN–EDGE ABSORPTION

Being at redshifts between 2 and $\sim$3.7, the optical–UV flux of the blazars in our sample could be affected by absorption of neutral hydrogen in intervening Lyman–α absorption systems. Single ionised helium is not an issue at these redshifts for UVOT wavelengths. Not knowing the real attenuation along individual line of sights, we estimate the *probable* attenuation using the effective opacity $\tau_{\rm eff} \equiv -\ln < {\rm e}^{-\tau} >$, where the average is taken over all possible line of sights. We compute the mean attenuation for six wavelengths approximately centred in the six UVOT filters. Fig. 3 shows the corresponding $\tau_{\rm eff}$ as a function of redshift. We adopt the column density distribution described in Haardt & Madau (in preparation), which is based on the mean free path measurements of Prochaska et al. (2009). Full details os our calculation will be described in Haardt et al. (in preparation), together with a more refined treatment of the mean attenuation and its variance around the mean. Such procedure is very crude, as the attenuation variance along an individual line of sight is large for a fixed observed wavelength. We must note however that: i) the variance of the attenuation is largely reduced when the actual filter width is taken into account (Madau 1995), and ii) the variance of the attenuation is mainly driven by the few Lyman limit systems present along an individual line of sight. Our absorption model results in a mean number of thick systems which is < 1 for $z \lesssim 4$, so we do note expect excessive off–set of the attenuation along individual line of sight with respect to the mean value.

When presenting the SED of our sources, we will show both the fluxes and upper limits de–reddened for the extinction due to our Galaxy and the fluxes (and upper limits) obtained by de–absorbing them with the $\tau_{\rm eff}$ shown in Fig. 3.

5 THE SPECTRAL ENERGY DISTRIBUTION

Although the SED of several blazars of our sample have already been presented in the literature, we show them all in Fig. 4–6, adding to the archival data the BAT data from the A09 catalogue. The SEDs show the following general properties:

- We show as a grey stripe the detection limits of the LAT instrument: the lower bound corresponds to the pre–flight differential sensitivity limit for one year survey at the 5 σ level[2], while the upper bound is simply a factor 4 higher. The latter should mimic the approximate sensitivity limit for the three months LAT survey at 10σ confidence level. These curves depend on the assumed spectral index of the source, and have been obtained assuming $\alpha_\gamma = 1$, approximately valid for the expected spectrum of FSRQs. All sources in the present sample have not been detected in the first 3–months LAT survey. Their γ–ray flux should then lie below the upper bound of the grey stripe. This, together with the BAT data, constrains the high energy peak of the SED to occur in the MeV band. Two blazars, 0537–286 and 0836+710, were detected by EGRET (Nandikotkur et al. 2007; Thompson et al. 1993) with a flux level reported in Fig. 4 and Fig. 5. This indicates a large variability amplitude.
- The high energy peak is dominating the electromagnetic output with luminosities exceeding 10^{48} erg s^{-1} in all cases but S5 0014+813 (in which it is the accretion disk luminosity that dominates the power output).
- The 0.3–10 keV *Swift*/XRT data indicate a very hard X–ray spectrum, harder than the BAT one, but, in general, the extrapolation from the XRT agrees with the BAT flux. The BAT spectrum is a three–years average, while the XRT spectrum is more often a one–epoch spectrum, and rarely an average of the available observations.
- In the optical–UV band the spectrum is almost always steep (exceptions are 1210+330 and 225155+2217), and sometimes shows a peak. This component can be interpreted as the emission from the accretion disk (see G10; Ghisellini et al. 2009, and §4.2).
- When there are multiple X–ray observations, these show variability, with an apparent tendency for a "harder when brighter" behaviour of the X–ray flux (see 0222+185; 0836+710; 2126–158; 2149–306 and 225155+2217). The variability amplitude thus is greater at higher energies, being very modest below a few keV.

5.1 The model

To model the SED we have used a relatively simple leptonic, one–zone synchrotron and inverse Compton model. This model, fully discussed in Ghisellini & Tavecchio (2009), has the following main characteristics.

We assume that in a spherical region of radius R, located at

[2] see: http://fermi.gsfc.nasa.gov/ssc/data/analysis/documentation/Cicerone/Cicerone_LAT_IRFs/

source	OBS date dd/mm/yyyy	$t_{\rm exp}$ s	$N_{\rm H}^{\rm Gal}$ 10^{20} cm^{-2}	Γ_1	Γ_2	$E_{\rm break}$ keV	$F_{0.3-10}^{\rm unabs}$ 10^{-12} cgs	χ^2 or $C_{\rm stat}$	dof
0014+81	sum$^{(a)}$	8311	13.6	1.32±0.1			5.4	22.6	19
0222+185	28/07/2006	4150	9.3	1.20±0.08			14±8	344	378
0537–286	08/12/2005	14737	2.2	1.20±0.08			4±0.1	333	407
074625+2549	05/11/2005	24999	4.6	1.22±0.06			4.6±0.2	467	543
0805+614	sum$^{(b)}$	8121	4.7	1.25±0.13			3.14	10.8	10
0836+710	13/04/2007	7367	2.9	1.42±0.05			17.5±0.5	526	532
1210+330	26/10/2009	3782	1.16	1.9±0.37			0.57±0.15	31	41
2126–158	sum$^{(c)}$	34782	5.0	0.6±0.3	1.5±0.05	0.95±0.2	10.3	204	161
2149–306	10/12/2005	3336	1.6	1.45±0.07			16.2±8	367	394
225155+2217	22/05/2007	12396	5.0	1.28±0.08			4.66	19	25

Table 2. Results of the X–ray analysis. (a) sum of the observations 11/01/2007, 12/01/2007 and 14/01/2007; (b) sum of the observations 23/01/2009, 17/10/2006 and 21/01/2009; (c) sum of the observations 07/04/2007, 21/11/2008 and 06/04/2007.

Source	A_V	v	b	u	$uvw1$	$uvm2$	$uvw2$
0014+81	0.70	16.43 ± 0.05	17.57 ± 0.06	18.2 ± 0.1	> 19.4	> 19.6	> 20.0
0222+185	0.916	18.62 ± 0.25	19.28 ± 0.13	19.35 ± 0.18	> 20.65	...	> 20.85
0537–286	0.125	19.39 ± 0.1	19.94 ± 0.07	21.05 ± 0.19	> 22.25	> 22.31	> 22.82
074625+2549	0.12	19.42 ± 0.14	19.84 ± 0.14	20.09 ± 0.17	> 21.6	> 21.89	> 22.37
0805+6144	0.189	> 19.3	> 20.4	> 20.1	> 20.5	> 20.3	> 20.4
0836+710	0.101	17.17 ± 0.05	17.29 ± 0.03	16.46 ± 0.02	17.34 ± 0.03	17.88 ± 0.05	17.21 ± 0.04
1210+330	0.041	19.01 ± 0.25	18.97 ± 0.11	18.78 ± 0.12	19.38 ± 0.14	19.00 ± 0.11	20.13 ± 0.17
2126–158	0.264	17.03 ± 0.06	18.20 ± 0.06	19.5 ± 0.2	> 19.8	> 20.3	> 20.6
2149–306	0.083	17.66±0.08	17.88 ± 0.06	17.33 ± 0.05	18.31 ± 0.08	20.44 ± 0.24	20.21 ± 0.13
225155+2217	0.272	...	...	> 20.7	> 22.0	> 22.2	> 21.2

Table 3. Summary of *Swift*/UVOT observed magnitudes. Lower limits are at 3σ level. Values of A_V from Schlegel et al. (1998).

a distance $R_{\rm diss}$ from the central black hole, relativistic electrons are injected at a rate $Q(\gamma)$ [cm^{-3} s^{-1}] for a finite time equal to the light crossing time R/c. For the shape of $Q(\gamma)$ we adopt a smoothly broken power law, with a break at $\gamma_{\rm b}$:

$$Q(\gamma) \, = \, Q_0 \, \frac{(\gamma/\gamma_{\rm b})^{-s_1}}{1+(\gamma/\gamma_{\rm b})^{-s_1+s_2}} \qquad (2)$$

The emitting region is moving with a velocity βc corresponding to a bulk Lorentz factor Γ. We observe the source at the viewing angle $\theta_{\rm v}$ and the Doppler factor is $\delta = 1/[\Gamma(1-\beta\cos\theta_{\rm v})]$. The magnetic field B is tangled and uniform throughout the emitting region. We take into account several sources of radiation externally to the jet: i) the broad line photons, assumed to re–emit 10% of the accretion luminosity from a shell–like distribution of clouds located at a distance $R_{\rm BLR} = 10^{17} L_{\rm d,45}^{1/2}$ cm; ii) the IR emission from a dusty torus, located at a distance $R_{\rm IR} = 2.5 \times 10^{18} L_{\rm d,45}^{1/2}$ cm; iii) the direct emission from the accretion disk, including its X–ray corona; iv) the starlight contribution from the inner region of the host galaxy; v) the cosmic background radiation. All these contributions are evaluated in the blob comoving frame, where we calculate the corresponding inverse Compton radiation from all these contributions, and then transform into the observer frame.

We calculate the energy distribution $N(\gamma)$ [cm^{-3}] of the emitting particles at the particular time R/c, when the injection process ends. Our numerical code solves the continuity equation which includes injection, radiative cooling and $e^{\pm}$ pair production and reprocessing. Our is not a time dependent code: we give a "snapshot" of the predicted SED at the time R/c, when the particle distribution $N(\gamma)$ and consequently the produced flux are at their maximum.

Since we are dealing with very powerful sources, the radiative cooling time of the particles is short, shorter than R/c even for the least energetic particles. This implies that, at lower energies, the $N(\gamma)$ distribution is proportional to γ^{-2}, while, above $\gamma_{\rm b}$, $N(\gamma) \propto \gamma^{-(s_2+1)}$. The electrons emitting most of the observed radiation have energies $\gamma_{\rm peak}$ which is close to $\gamma_{\rm b}$ (but these two energies are not exactly equal, due to the curved injected spectrum).

We model at the same time the thermal disk (and IR torus) radiation and the non–thermal jet–emission. The link between these two components is given by the amount of radiation energy density (as seen in the comoving frame of the emitting blob) coming directly from the accretion disk or reprocessed by the BLR and the IR torus. This radiation energy density depends mainly on $R_{\rm diss}$, but not on the adopted accretion rate or black hole mass (they are in any case chosen to reproduce the observed thermal disk luminosity).

To calculate the flux produced by the accretion disk, we adopt a standard Shakura & Sunyaev (1973) disk (see Ghisellini & Tavecchio 2009). This allow us to fit also the thermal radiation seen in the optical–UV range, and to estimate the accretion rate and the black hole mass, as discussed below.

5.2 Estimate of the black hole mass

For all our sources, we interpret the near–IR, optical and UV emission as due to the accretion disk. For simplicity, we assume

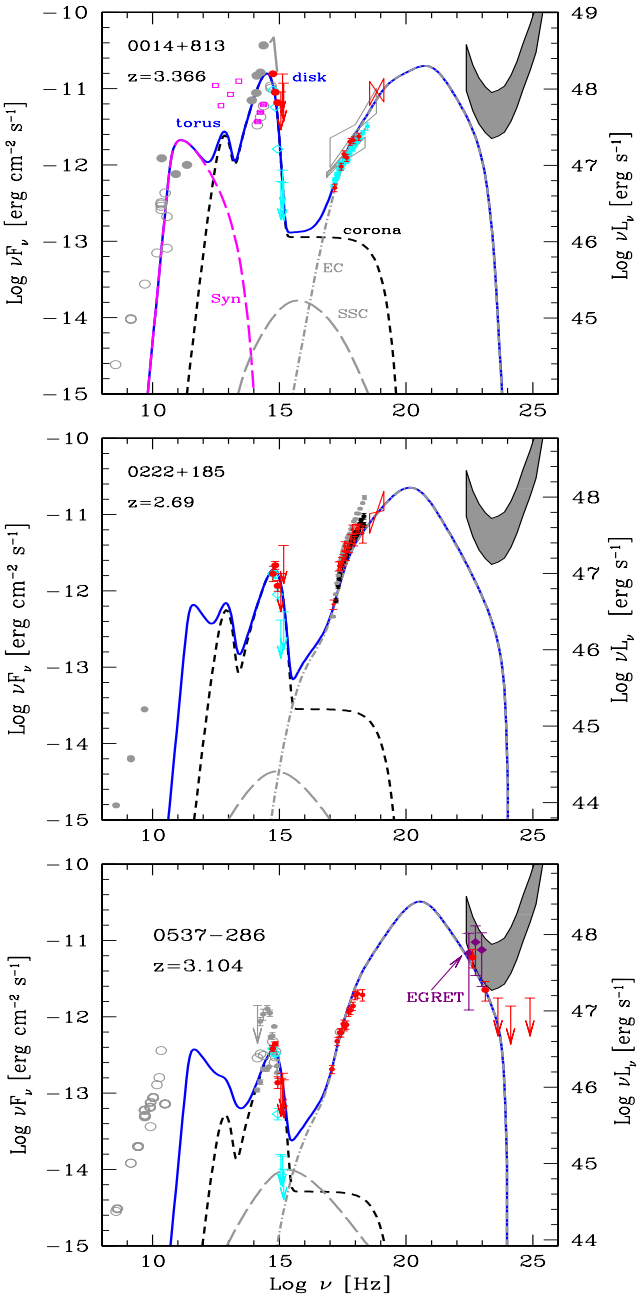

Figure 4. SEDs of S5 0014+813, 0222+185 (=RBS 315) and PKS 0537–286 together with the fitting models, with parameters listed in Tab. 4. De–absorbed UVOT, XRT and BAT data are indicated by darker symbols (red in the electronic version), while archival data (from NED) are in light grey. Diamonds (and lower arrows, cyan in the electronic version) indicate UVOT data not de–absorbed by intervening Lyman–α clouds. The magenta square symbols for S5 0014+813 are IRAS and 2MASS data points. The short–dashed line is the emission from the IR torus, the accretion disk and its X–ray corona. The long dashed and the dot–dashed grey lines are the synchrotron self–Compton (SSC) and the External Compton (EC) components, respectively. The thick solid (blue) line is the sum of all components.

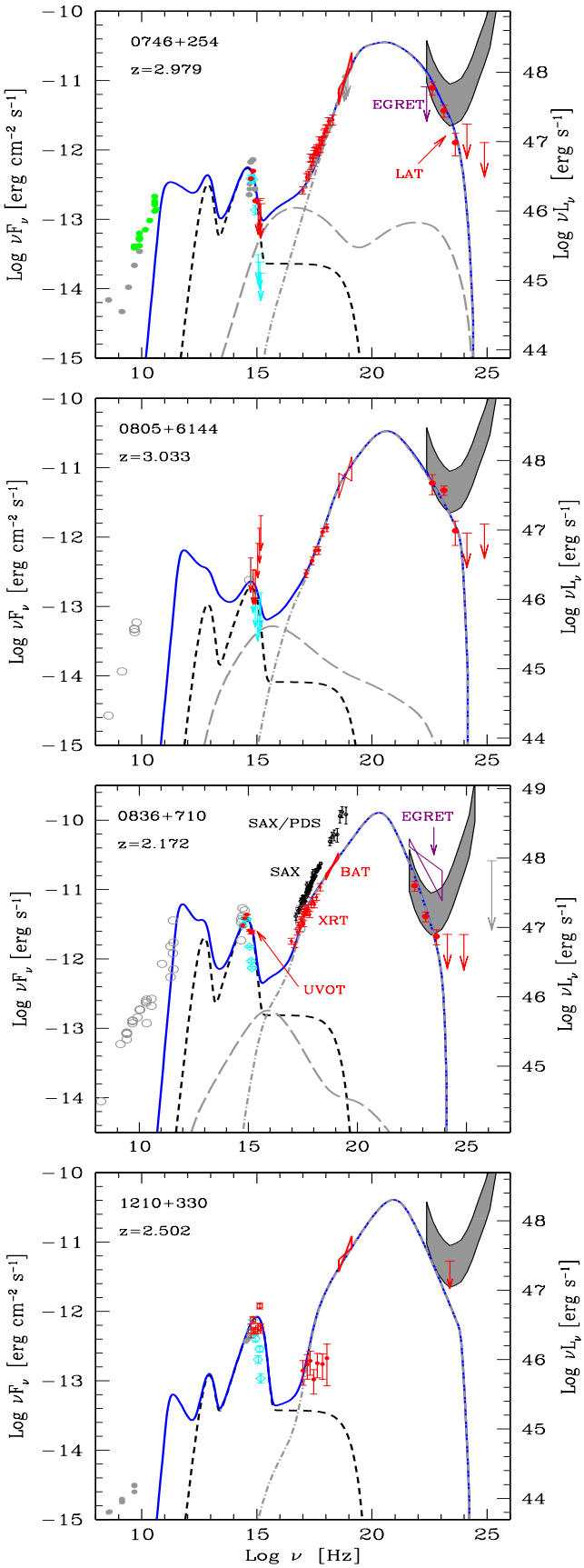

Figure 5. SED of SDSS 074625+2549, PKS 0805-6144, PKS 0836+710 and B2 1210+330. Symbols and lines as in Fig. 4.

that the disk is an optically thin, geometrically thick, Shakura–Sunjaev (1973) disk, emitting a black-body at each radius. The maximum temperature (and hence the νF_ν peak of the disk luminosity) occurs at $\sim$5 Schwarzschild radii and scales as $T_{\rm max} \propto (L_{\rm d}/L_{\rm Edd})^{1/4} M^{-1/4}$. The total optical–UV flux gives $L_{\rm d} = \eta \dot{M} c^2$. Once we specify the efficiency η, we can derive both the

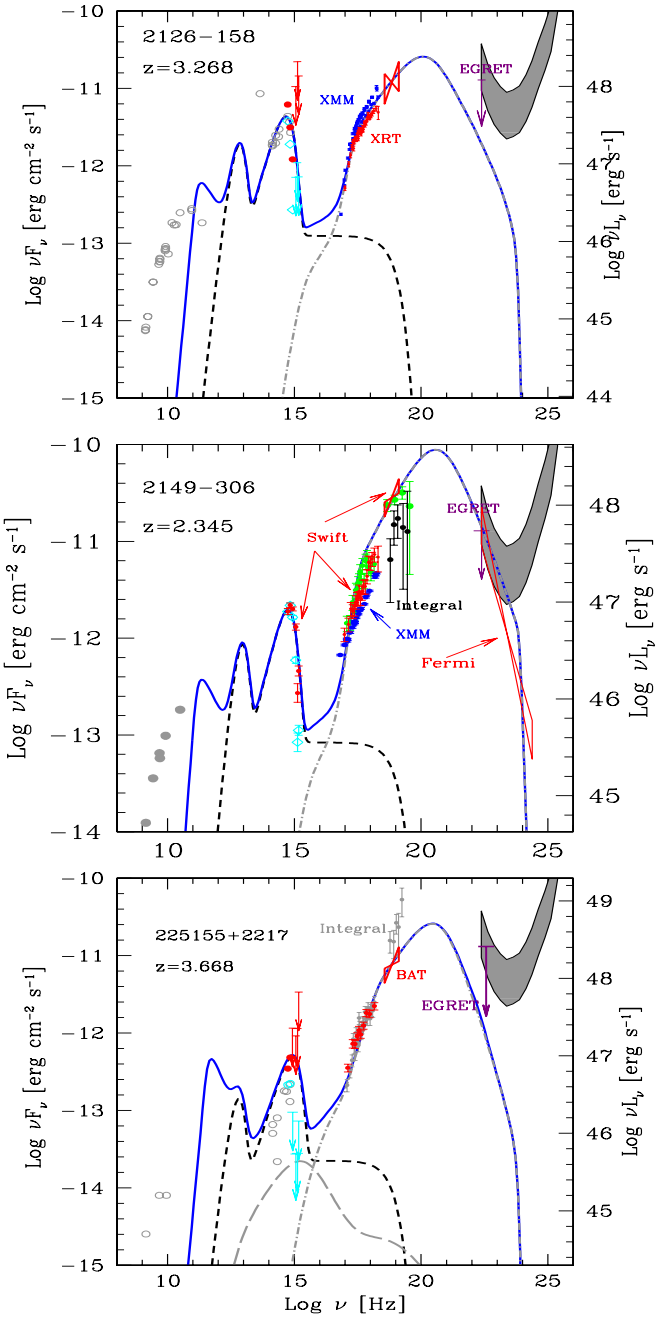

Figure 6. SED of PKS 2126–158, PKS 2149–306 and MG3 J225155+2217. Symbols and lines as in Fig. 4.

black hole mass and the accretion rate. Assuming a Schwarzschild black hole, we set $\eta = 0.08$.

In Fig. 7 we show a zoom of the SED of PKS 2149–306, to illustrate the uncertainties on the estimated value of the mass of the central black hole. The three SEDs shown correspond to $M = 3\times10^9$, 5×10^9 and 10^{10} solar masses. The maximum temperature of the accretion disk is a (albeit weak) function of the black hole mass: the overall disk emission becomes bluer for smaller black hole masses. From Fig. 7 one can see that the $M = 3\times10^9 M_\odot$ case gives a poor fit, while the $M = 10^{10} M_\odot$ case tends to overproduce the flux at lower optical frequencies. We can conclude that, within our assumptions and when the data show the peak of the thermal emission, the resulting estimate of the black hole mass is rather accurate with uncertainties that are significantly smaller than a factor 2.

Three caveats are in order. The first is that we are assuming a standard Shakura & Sunjaev (1973) disk, namely a disk geometrically thin and optically thick, emitting black–body radiation at each annulus according to a standard temperature profile (e.g. Frank, King & Raine 2002). For very large accretion rates, close to Eddington, the disk structure might be modified, and in the inner region a funnel may develop, as in the so called "thick" and "slim" disks (see e.g. Abramowicz et al. 1988; Madau 1988; Szuszkiewicz, Malkan, & Abramowicz 1996) We have discussed this possibility for S5 0014+813 (Ghisellini et al. 2009). If a funnel is present, the emitted disk radiation is not isotropic any longer, and face–on observers (as for blazars) would see an amplified radiation, and this would lead to overestimate the black hole mass. We will discuss again this point later.

The second caveat concerns the assumption of a Schwarzschild, non rotating black hole. The efficiency η for a Kerr hole and corotating accretion disk is larger, as are the temperatures of the innermost radii. But also gravitational light bending and redshift are larger, and the calculation of the observed spectrum is not as straightforward as in the Schwarzschild case (see e.g. Li et al. 2005). Comparing the spectra calculated in the Schwarzschild and maximal Kerr case, for equal mass and accretion rate, and assuming that the disk emits black–body spectra at all radii, we have that the overall disk emission in the Kerr case is bluer and stronger above the emission peak, and very similar below (smaller frequencies are emitted at larger radii, where the emitted flux is insensitive to the black hole rotation). Decreasing the accretion rate would decrease the emission peak (because the maximum temperature would be smaller), but also the overall flux, both below and beyond the emission peak. Since we end up having a deficit in the low frequency part of the spectrum, we must change also the mass, in the direction of an *increase* of it, because this allows to have a smaller maximum temperature. Therefore, to recover the original SED in the case of a Kerr hole, we must decrease the accretion rate and increase the mass. So assuming Kerr holes would not help in decreasing the derived masses.

The third caveat is that the assumption of a black–body spectrum may be too simplistic: for some regions of the disk a modified black–body may be a better choice. Since a modified black–body is a less efficient radiator than a pure black–body, the resulting spectrum, for the same accretion rate and black hole mass, will be less powerful and bluer (because the disk will be hotter). If this occurs, then our derived black hole masses should be considered as lower limits.

6 RESULTS

Table 4 lists the parameters used to fit the SED of the 10 blazars. We find that they are all distributed in a narrow range, as expected, because we are dealing with extremely powerful objects, characterised by similar (albeit extreme) properties.

The distance from the black hole, $R_{\rm diss}$, where dissipation occurs and most of the observed radiation is produced, ranges from 500 to 1.4×10^3 Schwarzschild radii. Three sources (0746+253, 1210+330 and marginally 2149–306) have $R_{\rm diss} > R_{\rm BLR}$, while for all the others the location of the dissipation region lies within the BLR.

The injected power in the form of relativistic electrons is very similar, around 10^{44} erg s^{-1} for all sources, and since the cooling

Name [1]	z [2]	$R_{\rm diss}$ [3]	M [4]	$R_{\rm BLR}$ [5]	$P'_{\rm i}$ [6]	$L_{\rm d}$ [7]	B [8]	Γ [9]	$\gamma_{\rm b}$ [10]	$\gamma_{\rm max}$ [11]	s_1 [12]	s_2 [13]
0014+813	3.366	9.6e3 (800)	4e10	5.5e3	0.12	3e3 (0.5)	0.33	16	150	2e3	–1	3
0222+185	2.69	660 (550)	4e9	1.45e3	0.08	210 (0.35)	2.94	13.5	40	2e3	0	3.2
0537–286	3.104	420 (700)	2e9	735	0.13	54 (0.18)	1.92	15	50	2e3	–1	3
0746+254	2.979	1.65e3 (1.1e3)	5e9	866	0.24	75 (0.1)	0.1	15	200	5e3	0.75	2.6
0805+614	3.033	270 (600)	1.5e9	581	0.15	34 (0.15)	2.54	14	60	3e3	–0.5	3
0836+710	2.172	540 (600)	3e9	1.5e3	0.22	225 (0.5)	3.28	14	90	2e3	–1	3.6
1210+330	2.502	420 (1.4e3)	1e9	866	0.08	75 (0.5)	0.73	16	80	3e3	–0.5	3.5
2126–158	3.268	1.8e3 (600)	1e10	2.7e3	0.13	750 (0.5)	2.61	14.1	40	2e3	0	3.3
2149–306	2.345	1.2e3 (800)	5e9	1.24e3	0.18	150 (0.2)	1.12	15	60	3e3	0	3.3
225155+2217	3.668	300 (1e3)	1e9	1.06e3	0.15	112 (0.75)	2.78	15	70	2e3	0	4
average	3	1.8e3 (1e3)	6e9	1.3e3	0.15	180 (0.2)	0.82	15	100	2e3	0	3
$\langle$LAT $z>2\rangle$	2.2	630 (700)	3e9	948	0.1	90 (0.2)	1.65	15	300	4e3	0	2.8

Table 4. List of parameters used to construct the theoretical SED. Col. [1]: name; Col. [2]: redshift; Col. [3]: dissipation radius in units of 10^{15} cm and (in parenthesis) in units of Schwarzschild radii; Col. [4]: black hole mass in solar masses; Col. [5]: size of the BLR in units of 10^{15} cm; Col. [6]: power injected in the blob calculated in the comoving frame, in units of 10^{45} erg s^{-1}; Col. [7]: accretion disk luminosity in units of 10^{45} erg s^{-1} and (in parenthesis) in units of $L_{\rm Edd}$; Col. [8]: magnetic field in Gauss; Col. [9]: bulk Lorentz factor at $R_{\rm diss}$; Col. [10] and [11]: break and maximum random Lorentz factors of the injected electrons; Col. [12] and [13]: slopes of the injected electron distribution [$Q(\gamma)$] below and above $\gamma_{\rm b}$; The total X–ray corona luminosity is assumed to be in the range 10–30 per cent of $L_{\rm d}$. Its spectral shape is assumed to be always $\propto \nu^{-1}\exp(-h\nu/150\ {\rm keV})$. The viewing angle $\theta_{\rm v}$ is 3° for all sources.

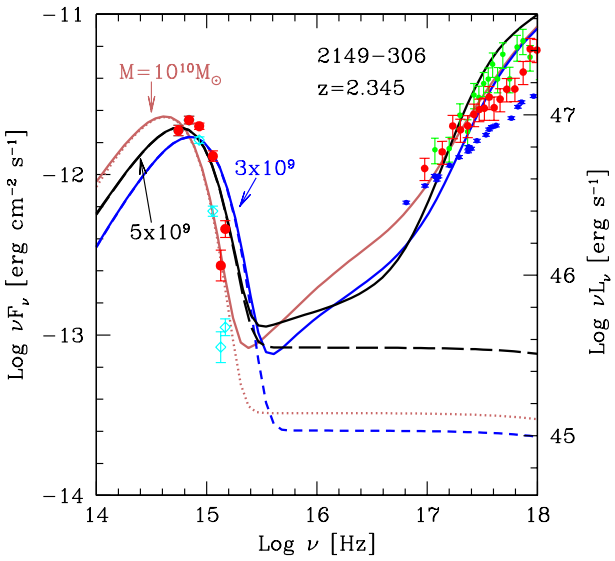

Figure 7. Zoom of the SED of PKS 2149–306, to show how the theoretical SED changes by changing the black hole mass. Three values are shown: $M=3\times10^9$, 5×10^9 and 10^{10} solar masses. Dotted, short and long dashed lines show the contribution of the accretion disk and its X–ray corona, while solid lines show the sum of the thermal and the beamed non-thermal components.

Name	$\log P_{\rm r}$	$\log P_{\rm B}$	$\log P_{\rm e}$	$\log P_{\rm p}$
0048–071	46.42	46.98	45.73	47.49
0222+185	46.11	46.42	45.27	47.89
0537–286	46.43	45.74	45.52	48.01
0746+253	46.53	44.36	46.28	47.85
0805+614	46.42	45.34	45.64	47.99
0836+710	46.60	46.36	45.54	48.00
1210+330	46.30	44.95	45.27	47.79
2126–158	46.38	47.27	45.12	47.84
2149–306	46.59	46.18	45.25	48.02
225155+2217	46.48	45.77	45.74	48.19
average	46.43	45.96	45.54	47.92
$\langle$LAT $z>2\rangle$	46.3	46.0	44.8	47.2

Table 5. Logarithm of the jet power in the form of radiation, Poynting flux, bulk motion of electrons and protons (assuming one proton per emitting electron). Powers are in erg s^{-1}.

is severe, all of it is transformed in radiation. The accretion disk luminosity is at the level of 0.1–0.4 $L_{\rm Edd}$, even if it spans a large range in absolute units, between 3×10^{46} and 2×10^{48} erg s^{-1}, due to the range of the black hole masses. The bulk Lorentz factor is between 13 and 18.

6.1 Comparison with bright Fermi/LAT blazars

It is instructive to compare the jet power and accretion disk luminosities of the BAT blazars of our sample with all the bright blazars detected by the LAT 3–months survey, as analysed in G10. The jet carries power in the form of bulk motion of particles (electrons and protons) and magnetic field. Furthermore, we can calculate the power spent by the jet to produce the radiation we see. The different components of the jet power are

$$P_i \ = \ \pi r_{\rm diss}^2 \Gamma^2 \beta c U'_i \qquad (3)$$

where U'_i is the energy density of the i component, as measured in the comoving frame. We define the total jet power as the sum of the electron ($P_{\rm e}$), proton ($P_{\rm p}$), found assuming one proton per electron, and magnetic field ($P_{\rm B}$) contributions, while we call $P_{\rm r}$ the power spent in producing radiation. Table 5 lists the jet powers for the 10 BAT blazars.

$P_{\rm r}$ vs $L_{\rm d}$ — Fig. 8 shows $P_{\rm r}$ as a function of the accretion luminosity $L_{\rm d}$ for our BAT blazars, together with all the LAT blazars in G10. These include BL Lac objects for which only an up-

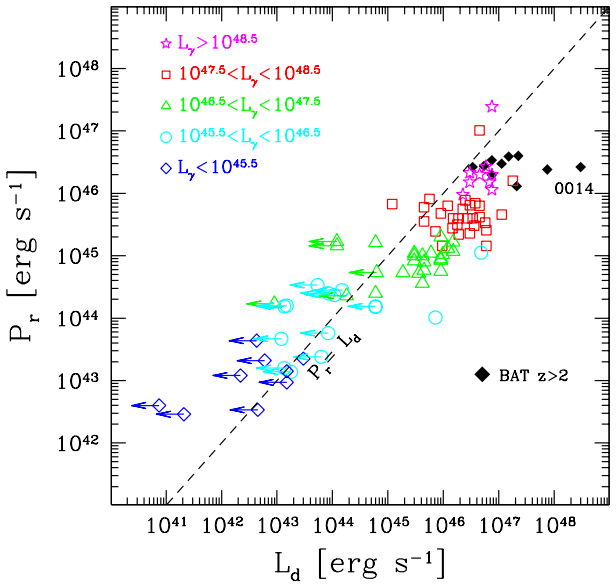

Figure 8. The power spent by the jet to produce the radiation we see, $P_{\rm r}$, as a function of the accretion disk luminosity $L_{\rm d}$. BAT blazars (black diamonds) are compared with the blazars in the *Fermi* 3–months catalogue of bright sources detected above 100 MeV. The latter have different symbols according to their γ–luminosity, as labelled.

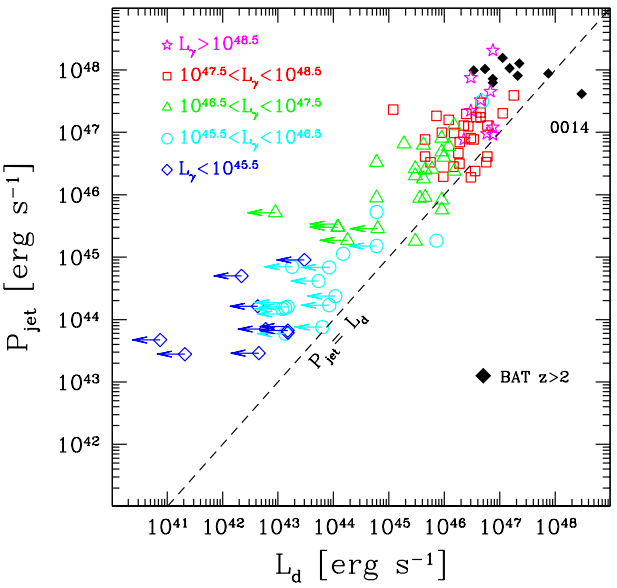

Figure 9. The jet power $P_{\rm jet}$ as a function of the accretion disk luminosity $L_{\rm d}$. Symbols as in Fig. 8.

per limit to their disk luminosity could be found (shown by arrows). Black filled diamonds correspond to the BAT blazars. The power $P_{\rm r} = \pi r_{\rm diss}^2 \Gamma^2 \beta c U'_{\rm rad}$, can be re–written as [using $U'_{\rm rad} = L'/(4\pi r_{\rm diss}^2 c)$]:

$$P_{\rm r} = L' \frac{\Gamma^2}{4} = L \frac{\Gamma^2}{4\delta^4} \sim L \frac{1}{4\delta^2} \qquad (4)$$

where L is the total observed non–thermal luminosity (L' is in the comoving frame) and $U'_{\rm rad}$ is the radiation energy density produced by the jet (i.e. excluding the external components). The last equality assumes $\theta_{\rm v} \sim 1/\Gamma$. This quantity is almost model–independent,

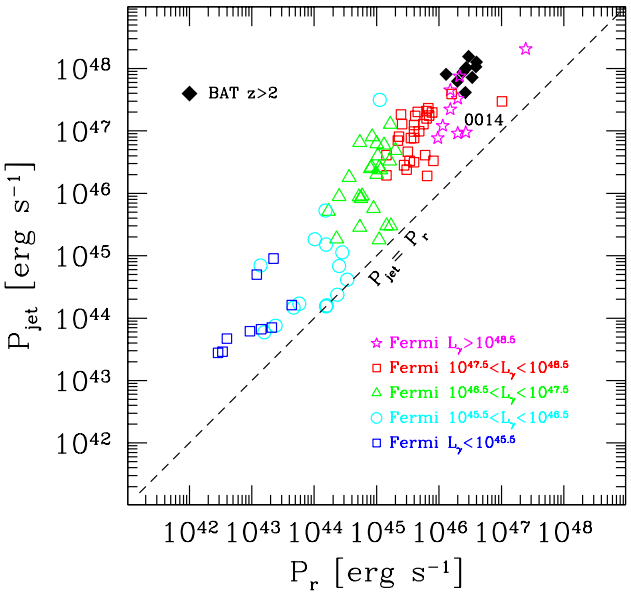

Figure 10. The jet power $P_{\rm jet}$ as a function of the power spent by the jet to produce the radiation we see, $P_{\rm r}$. Symbols as in Fig. 8

since it depends only on the adopted δ, that can be estimated also by other means, namely superluminal motions. Therefore Fig. 8 shows two quantities that are (almost) model–independent. The BAT blazars are the most extreme, lying at the upper end of the $P_{\rm r}$–$L_{\rm d}$ distribution. All follow the trend defined by the LAT FSRQs, with the exception of S5 0014+813, that has an accretion disk luminosity larger than what expected from its jet luminosity.

$P_{\rm jet}$ vs $L_{\rm d}$ — Fig. 9 shows the jet power $P_{\rm jet} = P_{\rm p} + P_{\rm e} + P_{\rm B}$ as a function of the disk luminosity. Again, the BAT blazars have the most powerful jets and disks, and S5 0014+813 appears to be an outlier with respect to the general trend defined by the ensemble of LAT and BAT blazars.

$P_{\rm jet}$ vs $P_{\rm r}$ — Fig. 10 shows the jet power as a function of $P_{\rm r}$, the power in radiation. It shows the efficiency of the jet in converting its bulk power into radiation. Low power BL Lacs are the most efficient in converting $P_{\rm jet}$ into $P_{\rm r}$, while powerful blazars are less efficient. The BAT blazars follows this trend, and in this plot S5 0014+813 is not an outlier.

This suggests that S5 0014+813 indeed has an over–luminous accretion disk with respect to its jet, and this favours the hypothesis, discussed in Ghisellini et al. (2009) that the thermal radiation from the inner parts of the disk is geometrically collimated by the presence of a funnel, possibly as a consequence of the large accretion rate in Eddington units (likely to be even larger than what calculated here and in Ghisellini et al. 2009, because we assumed a standard disk).

For the other BAT blazars, instead, there is no need to invoke a non–standard accretion disk, since they follow the jet power – disk luminosity relation defined by less extreme blazars, selected from the *Fermi*/LAT survey. The latter have luminosities around 0.1 of the Eddington one or even less, and should indeed have standard disks. This suggests that the black hole masses estimated for the other BAT blazars are robust, and not a consequence of our assumption of a standard accretion disk.

It is then interesting to compare the black hole masses derived for our BAT blazars with those of the 3–months survey of LAT, and

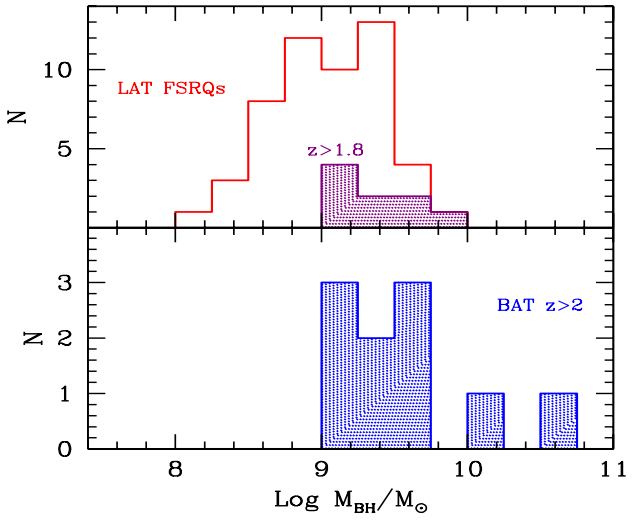

Figure 11. Comparison of black hole mass distributions. The top panel shows all *Fermi*/LAT FSRQs (i.e. excluding BL Lacs), and the 9 *Swift*/BAT FSRQs with $z > 1.8$. The bottom panel shows the mass distribution of the 10 BAT blazars at $z > 2$.

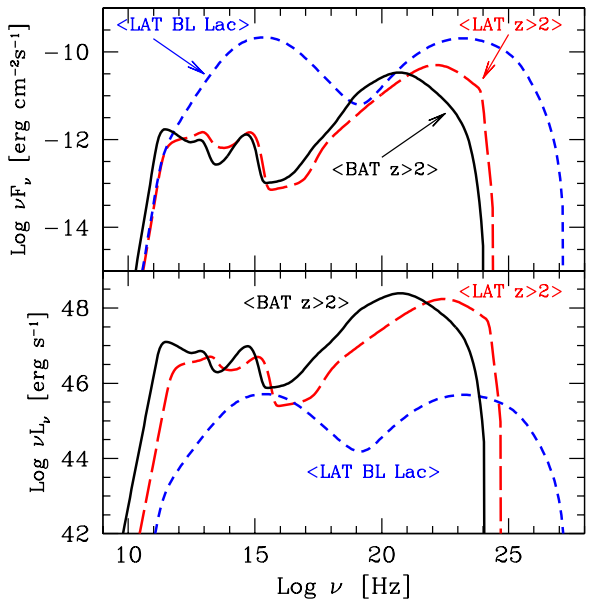

Figure 12. Average SEDs for the sources in our samples, for all FSRQs detected by *Fermi* and for the subsample of the 8 *Fermi*–blazars at redshift $z > 1.8$). The top and the bottom panels show the fluxes and luminosities, respectively. The shown frequencies are calculated in the rest frame of the source for the luminosity plot, and are the observed ones for the flux plot. In Tab. 4 we list the parameters used to construct the shown SEDs for FSRQs, while, for the LAT BL Lacs, we report the same SED as shown in G10.

then to the sub–sample (of 9 objects) of LAT blazars at $z > 1.8$. This is done in Fig. 11: high redshift BAT blazars have a black hole mass distribution extending to larger values than the high–z LAT blazars. The numbers are too small for a statistical comparison, and a K–S test returns a large probability that the two distributions are drawn from the same one. In any case, we can safely conclude that the hard X–ray selection is a very efficient way to pinpoint the most powerful extreme of the blazar population, possibly more than selecting them through their *Fermi*/LAT γ–ray flux. We can wonder if this merely depends on the sensitivities of the current BAT and LAT instruments, or if indeed the most powerful blazar jets are more luminous in hard X–rays than in the 0.1–10 GeV band. In Fig. 12 we try to answer to this question by showing three theoretical SEDs corresponding to; i) the average SED of BL Lacs detected by the 3–months LAT survey (see the used parameters in G10); ii) the average SED of the $z > 2$ FSRQs detected by the same LAT survey, and iii) the average SED of our $z > 2$ BAT FSRQs. For the latter two SEDs we used the parameters listed at the end of Tab. 4. We show both the flux (top panel) and the luminosity (bottom) SEDs. The shown frequencies are calculated in the rest frame of the source for the luminosity plot, and are the observed ones for the flux plot. Fig. 12 shows that:

- LAT BL Lacs and high redshift FSRQs have the same average flux in hard X–rays;
- LAT BL Lacs are on average brighter than high–z FSRQs in γ–rays;
- Comparing high redshift LAT and BAT FSRQs, we see that the latter are fainter in γ–rays and in fact none of our 10 BAT blazars has been detected in the 3–months LAT survey;
- In the luminosity plot, LAT BL Lacs are the least luminous (most of them are at $z < 0.5$, see Fig. 1);
- Comparing high–z BAT and LAT FSRQs, we see that BAT blazars are slightly more luminous (in bolometric terms) even if they are less powerful γ–ray sources. In the entire X–ray band they are more powerful than LAT blazars.

We have checked if some of the high redshift LAT and BAT blazars are present on the SDSS survey, with their black hole mass estimated through the FWHM of the emission lines and the ionising continuum luminosity. In the compilation of Shen et al. (2008) we have found RGB J0920+446 ($z = 2.190$) with different mass estimates, ranging from $M = 2 \times 10^9 M_\odot$ and $5 \times 10^{10} M_\odot$, to be compared with our estimate of $M = 6 \times 10^9 M_\odot$ (Ghisellini, Tavecchio & Ghirlanda 2009); 4C +38.41 (=1633+382, $z = 1.814$) with a mass in the range $(1.6 - 8) \times 10^9 M_\odot$ (our estimate: $M = 5 \times 10^9 M_\odot$, Ghisellini, Tavecchio & Ghirlanda 2009) and J074625.87+2549 with $M = 6 \times 10^9 M_\odot$ (our estimate: $M = 7 \times 10^9 M_\odot$, see Tab. 4). Also PKS 1502+106 ($z = 1.839$) is present in the SDSS (DR7) catalogue, but with no mass estimate yet.

All this phenomenology can be understood in simple terms on the basis of the blazar sequence: the most powerful blazars are FSRQs whose synchrotron peak is located in the sub–mm band, and whose high energy peak is located in the MeV band. So the 0.1–10 GeV luminosity, being in a band relatively far from the peak, is not very large. On the contrary, instruments sensitive in the hard X–ray band can catch these sources at their emission peak, making this band the optimal one in finding the upper end of the blazar luminosity distribution.

7 DISCUSSION

One of our major result is that *all* the 10 BAT blazars studied here have a black hole heavier than 10^9 solar masses. Among the BAT blazars they are the most luminous (all of them have $L_X > 2 \times 10^{47}$ erg s^{-1}) and the most distant (all of them have $z > 2$). Since these objects are at high redshifts, our finding has important implications on the number density of heavy black holes, especially if we consider that for each blazar pointing at us, there must be hundreds

of similar sources (having black holes of similar masses) pointing elsewhere. Using a mix of simple theoretical and observational considerations we will find in the following what we consider a conservative "minimal mass function" for heavy black holes associated to radio–loud objects. But before doing this we first discuss the implications of our results for future hard X–ray missions.

7.1 Implications for future missions

NHXM – The *New Hard X–ray Mission (NHXM)*[3] is a project for a satellite hosting 4 mirror modules able to concentrate X–ray photons in the 0.2–80 keV range (Pareschi et al. 2009). This is achieved in part by a long (10 meter) focal length and partly by a multi–layer coating. A 2–30 keV polarimeter is foreseen at the focus of one of the mirror modules. The angular resolution is better than $20''$ at 30 keV. The sensitivity above 10 keV is 2–3 orders of magnitude better than anything already flown. On the other hand, the long focal length limits the field of view to $\sim 12' \times 12'$.

The main contribution of this mission to the issue of finding large black hole masses at high redshift is to observe pre–selected candidates in the hard X–ray region of the spectrum, and consequently to assess the non–thermal nature of this emission. By establishing a large jet power, it will hint to a corresponding large accretion rate and thus a large black hole mass. In this context, we stress that the blazars we have analysed in this paper are all strong (> 0.1 Jy) radio sources and very hard in the "classical" 2–10 keV band. These properties can then be taken as selection criteria to construct a useful sample of radio–loud sources to be observed by $NHXM$.

EXIST – The *Energetic X–ray Imaging Survey Telescope (EXIST)*[4] is a proposed *Medium Class Mission* to conduct the most sensitive full–sky survey for black holes on all scales (from the stellar to the supermassive ones). To this purpose *EXIST* has been specifically designed to have onboard three complementary instruments:

- a large area (4.5 m^2), wide–field ($70^\circ \times 90^\circ$) hard X-ray (5–600 keV) imaging (2 arcmin resolution and $\sim 20''$ localisation for 5σ sources) coded mask telescope (HET, High Energy Telescope);
- a soft X-ray imager (SXI, focusing telescope with CCD, $\sim 2''$ localisations) operating over the 0.1–10 keV energy range with *XMM–Newton*–like (1–telescope) area;
- an optical/NIR telescope (IRT) with 1.1 m diameter with instruments covering the wavelength range 3000–22000 Å with R$\sim$3000 spectrograph and $4' \times 4'$ imaging array with objective prism capability.

HET has approximately a 20 times better sensitivity than BAT, and extends the energy range to lower and higher energies: it can then see powerful and distant blazars *at or very close to their peak of emission*. Furthermore, the operation mode (similar to *Fermi*), patrolling the entire sky every three hours, is ideal to discover rare objects. SXI can give crucial information about the level and shape of the 0.2–10 keV spectrum as well as to locate the X-ray sources on sky with an accuracy of few arcsec. Finally, IRT can take the IR and optical spectra (and/or photometry) of these rare sources, and can catch powerful blazars *where their accretion disk peaks*. Given the expected flux levels of IR–optical and X–ray fluxes of high redshift powerful blazars, these "follow–up" observations will be very inexpensive. *EXIST* has been designed to break the "multi-wavelength investigation bottleneck" by having on–board a suite of instruments on unprecedented wavelength coverage that operate simultaneously.

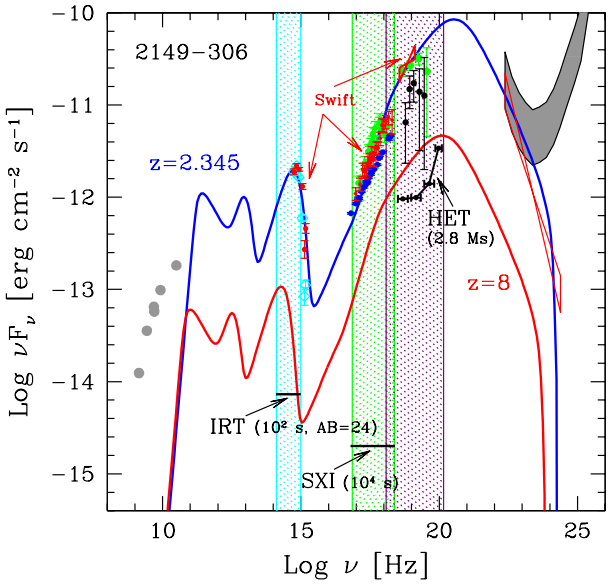

Figure 13. The SEDs and model for PKS 2149–306 at its actual redshift ($z = 2.345$) and what the model SED would appear if the source were at $z = 8$. We also show the limiting sensitivities for the three instruments foreseen to be onboard the *EXIST* mission: the high energy coded mask (HET, sensitive in the 5–600 keV range), the soft X–ray Telescope (SXI, operating in the 0.1–10 keV energy range), and the IR–optical telescope (IRT). We indicate the exposure time needed to reach the shown sensitivities. It is remarkable that powerful blazars like PKS 2149–306, if the existed even at $z = 8$, could easily be detected by hard X–ray telescopes like *EXIST*/HET. The presence of SXI and especially the IR–optical telescope would also allow to find the redshift and to very easily provide a complete spectrum of the accretion disk at its emission peak, thus yielding a robust estimate of the accretion rate and the black hole mass.

To illustrate these concepts, Fig. 13 shows the SED of PKS 2149–306, the theoretical fitting model, and the same model for a source located at $z = 8$ having the same total luminosity. We superimpose also the expected sensitivities of the three *EXIST* instruments (for the indicated exposure times). If blazars like PKS 2149–306 exist at high redshifts, *EXIST* will be able to find them and to characterise their general physical properties in a rather complete way. These include the jet power, the accretion disk luminosity and the black hole mass, that can be estimated in the same way as done in this paper.

Of course the choice of $z = 8$ (for Fig. 13) does not imply that blazars of this kind do exist at this redshift. To evaluate the number of blazars detectable by *EXIST* in the all sky survey we used the X–ray luminosity function and the cosmological evolution model of blazars as recently derived by A09 from the analysis of the BAT data. In particular, we used the modified pure luminosity evolution model with best fit parameters as reported in figure 9 of A09[5], re–normalising the luminosity function to the number of blazars detected by BAT (38 sources). A power–law spectrum with photon index equal to 1.5 has been assumed to convert the (15–55

[3] http://www.brera.inaf.it/NHXM2/
[4] http://exist.gsfc.nasa.gov/

[5] We used $\gamma_1 = -0.87$, $\gamma_2 = 2.73$, $L_\star = 1.8 \times 10^{44}$ erg s^{-1}, $k = 4.8$, $\gamma = -0.36$, see A09 for details.

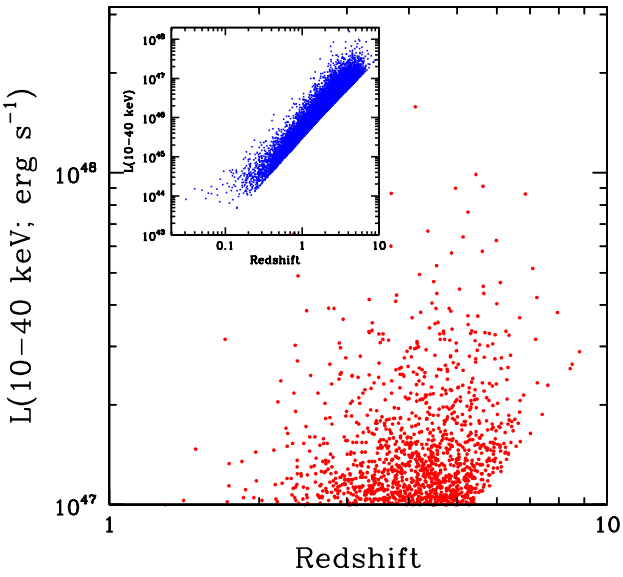

Figure 14. X–ray luminosity as a function of redshift for a simulated sample of blazars detectable by the two year all sky survey of *EXIST*. The inset shows the entire distribution, while the main figure zooms the region of high luminosity. This expected sample of blazars detectable by *EXIST* has been produced by extrapolating the cosmological evolution properties of the BAT blazars as derived by A09.

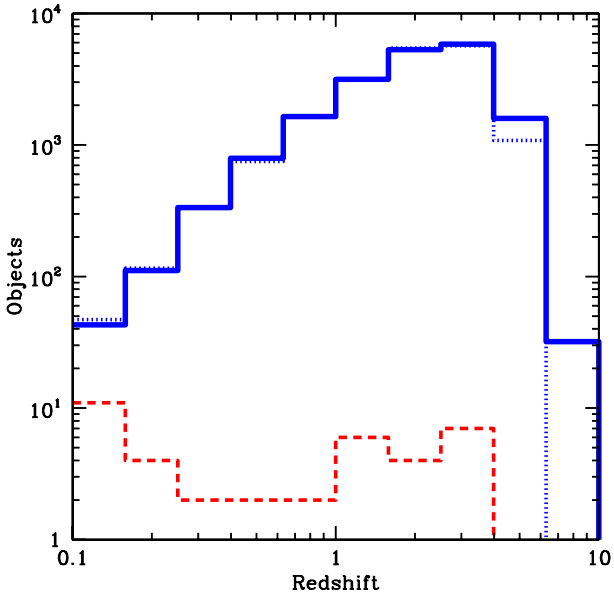

Figure 15. The redshift distribution of the blazars detectable by the 2 year all sky survey of *EXIST* compared with the redshift distribution of the BAT blazars (dashed line). The dotted histogram correspond to the "minimal" LF as discussed in the text.

keV) A09 luminosity function to the 10–40 keV energy range and to compute k-corrections.

Assuming a flux limit in the 10–40 keV energy band of $\sim 8 \times 10^{-13}$ erg cm^{-2} s^{-1} for the 2–years *EXIST* survey data, we expect $\sim 19,000$ blazars in the all sky survey. Their distribution in the luminosity–redshift plane is shown in Fig. 14, while their redshift distribution (compared with the redshift distribution of the BAT blazars) is shown in Fig. 15 (solid line). Table 6 list the expected number of blazars as a function of z, together with the number of high X–ray luminosity blazars possibly hosting a heavy black hole (columns 2 and 3, respectively). This makes it clear the great discovery potential of *EXIST*; more than 1500 blazars are expected at redshift greater than 4 and about a dozen at redshift greater than 7.

z	$N_{\rm A09}(>z)$	$L_X > L_{\rm thr}$	$N_{\rm min}(>z)$	$L_X > L_{\rm thr}$
0	1.9e4	223	1.83e4	121
1	1.6e4	223	1.53e4	121
2	1.0e4	222	9.7e3	120
3	4.9e3	199	4.3e3	102
4	1.6e3	154	1.0e3	57
5	335	76	41	5
6	58	24	1	0
7	11	9	0	0
8	3	3	0	0

Table 6. Number of blazars detectable by *EXIST* above a given redshift, according to the luminosity function derived in A09 and the limiting sensitivity of *EXIST* for the two year all sky survey. The third column gives the number of objects, above a given z and with X–ray luminosities above $L_{\rm thr} = 2 \times 10^{47}$ erg s^{-1}. The fourth and fifth column give the total number of blazars, and those exceeding $L_{\rm thr}$, for the "minimal" LF discussed in the text.

The expected number of high X–ray luminosity blazars reported in column 3 of Table 6 clearly depends on the extrapolation of the A09 cosmological evolution model at redshift greater than ~ 4, a redshift range where no BAT data are available. To derive a "strict" lower limit to the number of high X–ray luminosity blazars detectable by *EXIST* we have used a cosmological evolution model that is equal to the A09 one up to $z \sim 4.3$ (where they measure the peak of the density of high X–ray luminosity blazars) but having an exponential cutoff beyond $z = 4.3$ [$L_z = L_{z=4.3} \times \exp(z - 4.3)$ for $z > 4.3$]. This LF is consistent with the lower limits on the number of blazars known between $z = 4$ and $z = 5$ (see Fig. 16). In the following we will call this evolution model "minimal LF". The expected number of blazars computed using this "minimal LF" are reported in Table 6 (column 4 and 5), while their redshift distribution is shown in Fig. 15 (dotted line). As expected the only differences are at redshift greater than 4, where for this rather extreme "minimal LF" we expect to detect about 60 high X–ray luminosity blazars at $z > 4$, 5 at $z > 5$ and none at $z > 6$. The real number of high X–ray luminosity blazars detectable by *EXIST* are probably in–between the numbers reported in Table 6 (columns 3 and 5).

7.2 Black hole–dark halo connection at high redshifts

It is well known that growing a billion solar masses black hole within a billion years from the Big Bang is a challenge for hierarchical models of structure formation (e.g., Haiman 2004; Shapiro 2005; Volonteri & Rees 2005; Volonteri & Rees 2006; Tanaka 2009). Assuming accretion at the Eddington rate, a black hole mass increases in time as:

$$M(t) = M(0)\, \exp\left(\frac{1-\epsilon}{\epsilon}\frac{t}{t_{\rm Edd}}\right), \qquad (5)$$

where $t_{\rm Edd} = 0.45\,{\rm Gyr}$ and ϵ is the radiative efficiency. For a "standard" radiative efficiency $\epsilon \approx 0.1$, and a seed mass $M(0) = 10^2 - 10^4 M_\odot$, it takes at least 0.7–0.9 Gyr to grow up to $\simeq$

$10^{10} M_\odot$. The cosmic time at $z = 4$ is 1.5 Gyr, but it is only 0.9 Gyr at $z = 6$, and 0.7 Gyr at $z = 7$. We expect therefore that billion solar masses black holes at higher and higher redshift becomes increasingly rare.

We will provide an estimate of the number density of black holes with $M > 10^9 M_\odot$ as a function of redshift that is *independent* of the formation and growth efficiency of black holes. Empirical correlations have been found between the black hole mass (M) and the central stellar velocity dispersion (σ) of the host (Gültekin et al. 2009 and references therein), and between the central stellar velocity dispersion and the asymptotic circular velocity (V_c) of galaxies (Ferrarese 2002; Pizzella et al. 2005; Baes et al. 2003).

$$\sigma = 200\,\mathrm{km\,s^{-1}} \left(\frac{V_c}{320\,\mathrm{km\,s^{-1}}} \right)^{1.35} \quad (6)$$

and

$$\sigma = 200\,\mathrm{km\,s^{-1}} \left(\frac{V_c}{339\,\mathrm{km\,s^{-1}}} \right)^{1.04} \quad (7)$$

as suggested by Pizzella et al. (2005) and Baes et al. (2003), respectively.

The latter is a measure of the total mass of the dark matter halo of the host galaxies. A halo of mass M_h collapsing at redshift z has a circular velocity

$$V_c = 142\,\mathrm{km\,s^{-1}} \left[\frac{M_h}{10^{12}\,M_\odot} \right]^{1/3} \left[\frac{\Omega_m}{\Omega_m^z} \frac{\Delta_c}{18\pi^2} \right]^{1/6} (1+z)^{1/2} \quad (8)$$

where Δ_c is the over–density at virialization relative to the critical density. For a WMAP5 cosmology we adopt here the fitting formula (Bryan & Norman 1998) $\Delta_c = 18\pi^2 + 82d - 39d^2$, where $d \equiv \Omega_m^z - 1$ is evaluated at the collapse redshift, so that $\Omega_m^z = \Omega_m (1+z)^3 / (\Omega_m (1+z)^3 + \Omega_\Lambda + \Omega_k (1+z)^2)$.

We will further assume that the black hole–σ scaling is:

$$M = 10^9 M_\odot \left(\frac{\sigma}{356\,\mathrm{km\,s^{-1}}} \right)^4 . \quad (9)$$

and that these scaling relations observed in the local universe hold at all redshifts. Therefore we derive the relationship between black hole and dark matter halo mass (see also Bandara et al. 2009):

$$M_h = 4.1 \times 10^{13} M_\odot \left[\frac{M}{10^9 M_\odot} \right]^{0.56} \left[\frac{\Omega_m}{\Omega_m^z} \frac{\Delta_c}{18\pi^2} \right]^{-1/2} (1+z)^{-3/2} \quad (10)$$

and

$$M_h = 7.1 \times 10^{13} M_\odot \left[\frac{M}{10^9 M_\odot} \right]^{0.72} \left[\frac{\Omega_m}{\Omega_m^z} \frac{\Delta_c}{18\pi^2} \right]^{-1/2} (1+z)^{-3/2} \quad (11)$$

The number density of black holes with $M > 10^9 M_\odot$, therefore corresponds to the number density of halos with mass $M_h > M_{thr}$, if M_{thr} is the mass of a halo that hosts a billion solar masses black hole. We estimate the number density of dark matter halos using the Press & Schecter formalism (Sheth & Tormen 1999). In Fig. 16 we show the results as the grey stripe, encompassing the values found by the two methods above. This estimate ignores any issue related to black hole formation and growth timescale. The grey stripe can then be considered as a rough upper limit to the number density of heavy black holes as a function of redshift.

7.3 Large black hole masses at high redshift

These model predictions can be compared with the volume density of high redshift blazars hosting a black hole of mass larger than

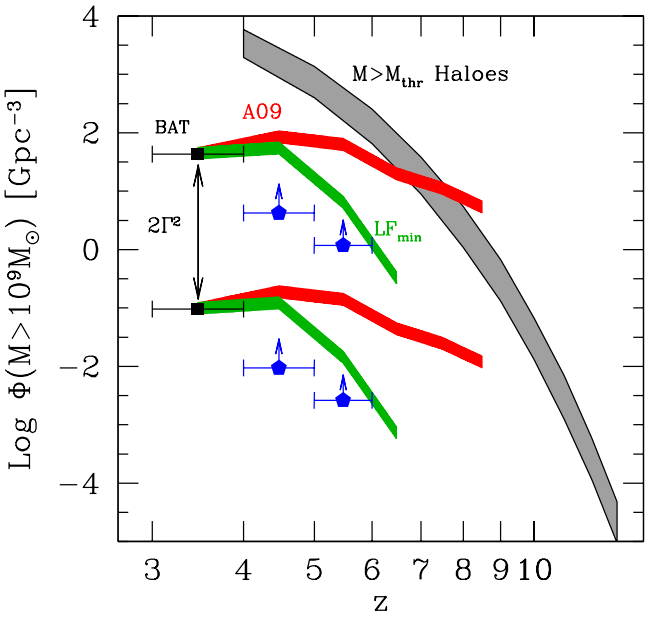

Figure 16. Number density of black holes with $M > 10^9 M_\odot$ as a function of redshift. The grey stripe is based purely on connecting black hole mass to halo mass (upper envelope: Pizzella et al. 2005; bottom: Baes et al. 2003) and estimating the number density of black holes via the number density of their host dark matter halos using the Press & Schecter formalism (see text). In the lower part of the figure we report, as grey stripes (red and green in the electronic version), the mass function $\Phi(z, M > 10^9 M_\odot)$ for blazars as derived from the luminosity function of A09, considering $L_X > 2 \times 10^{47}$ erg s^{-1}. These stripes correspond two "extreme" cases of cosmological evolution for the blazars population beyond redshift 4: the upper (red) stripe corresponds to the cosmological evolution model of A09 extrapolated up to $z \sim 9$, while the lower stripe corresponds to its "high–z cut-off version" as discussed in the text. The filled square in the $3 < z < 4$ bin is taken directly from Fig. 10 of A09. The filled pentagons and arrows are the lower limits derived from the existence of a few blazars in the 2 redshift bins. In the upper part of the figure we show the same points/stripes up–shifted by the factor $2\Gamma^2 = 450$, to account for misaligned sources. In this way the upper stripe of the mass function $\Phi(z, M > 10^9 M_\odot)$ for radio–loud sources is in conflict, at high z, with the estimates derived by massive halos, while the lower (green) stripe derived through the "minimal LF" is consistent.

$10^9 M_\odot$. The latter can be found using the cosmological evolution model of A09 along its high–z cut–off (i.e. "minimal") version (see §7.1), assuming, as we have found in this paper, that all blazars with $L_X > 2 \times 10^{47}$ erg s^{-1} have a $M > 10^9 M_\odot$ black hole. We cannot exclude that blazars with lower X–ray luminosity also host massive black holes, so the "observational" points, strictly speaking, are lower limits.

The lower part of Fig. 16 shows two stripes (red and green, in the electronic version) corresponding to two mass functions $\Phi(z, M > 10^9 M_\odot)$ of blazars, both calculated for X–ray luminosities larger than 2×10^{47} erg s^{-1}. The flatter (red) stripe corresponds to the cosmological evolution model of A09 extrapolated up to $z \sim 9$, while the steeper (green) stripe corresponds to its "high z cut-off version" ("minimal" LF, see §7.1 for details).

The lower limits shown with a (blue) pentagon and arrow in the 4–5 redshift bin corresponds to the existence of at least 4 blazars for which we have estimated a black hole mass larger than $10^9 M_\odot$. They are RXJ 1028.6–0844 ($z = 4.276$; Yuan et al. 2005); GB 1508+5714 ($z = 4.3$; Hook et al. 1995); PMN J0525–3343 ($z = 4.41$; Worsley et al. 2004a) and GB 1428+4217 ($z = 4.72$; Worsley

et al. 2004b). There are other 3 blazars with $4 < z < 5$ discussed in Yuan et al. (2006), but they have X–ray luminosities smaller than 10^{47} erg s^{-1}. The other lower limit shown by the (blue) pentagon and arrow in the 5–6 redshift bin corresponds to the existence of at least one blazar, Q0906+6930 at $z = 5.47$, with an estimated black hole mass of $2 \times 10^9 M_\odot$ (Romani 2006).

All these points concerns sources pointing at us. The real density of heavy black holes must account for the much larger population of misaligned sources. We have then multiplied the mass function $\Phi(z, M > 10^9 M_\odot)$ of blazars and the other lower limits by $2\Gamma^2 = 450$, i.e. we have assumed an average Γ–factor of 15, appropriate for the BAT blazars analysed here. Fig. 16 show the resulting points.

The mass function of heavy black holes of all jetted sources is now close or even greater (if we extend the cosmological evolution model of A09 beyond z$\sim$4) than the upper limit defined by "halo–black holes" (grey stripe) at the largest redshifts. The mass function derived by the "minimal" LF is instead consistent.

To summarise: the BAT blazar survey allowed to meaningfully construct the hard X–ray LF of blazars. We have shown that its high luminosity end can be translated into the mass function of black holes with more than one billion solar masses. Up to $z = 4$, where we do see blazars, the cosmological evolution model, as derived by A09, is secure. Beyond $z = 4$ it depends strongly on the assumed evolution. We have then constructed the minimal evolution consistent with the existing data and the (few) existing lower limits. As Fig. 16 shows, the true mass function of heavy black hole in jetted sources should be bracketed by the two shown mass functions derived from the A09 and the "minimal" LF. The true mass density should then lie in–between the two possible choices. The implications of this finding are far–reaching, and we plan to investigate them in a forthcoming study (Volonteri et al. in preparation).

8 CONCLUSIONS

We summarise here our main conclusions.

- In the α_X–L_X plane the ensemble of blazars detected by BAT separate quite clearly in BL Lac objects and FSRQs: the former have steeper spectra and lower luminosities. This is a manifestation of the blazar sequence, since low power blazars are characterised by a population of emitting electrons with a large energy break, implying larger synchrotron and Inverse Compton frequency peaks. In the hard X–ray range we often see, in BL Lacs, the steep synchrotron tail of emission, while in more powerful blazars (i.e. FSRQs), we see the hard Inverse Compton component.
- In the same plane there is an indication of a "divide", namely BL Lacs and FSRQs separate in luminosity, at a few times 10^{45} erg s^{-1}. This behaviour mirrors what occurs for *FERMI*/LAT blazars: the dividing luminosity indicates when the accretion disk changes mode of accretion, becoming radiatively inefficient for luminosities of the order of 0.3–1 per cent of the Eddington one.
- The 10 BAT blazars at $z > 2$ are among the most powerful known. Not only their beamed jet bolometric luminosity, but also their jet power and the accretion luminosities are among the largest ones.
- The black hole masses are also very large, to account for the observed disk luminosities and spectra. They are all greater than one billion solar masses and a few approach 10 billions.
- The "record holder" S5 0014+813, having a black hole mass of 40 billion solar masses, is an outlier with respect to the jet power – disk luminosity correlation defined by the *Fermi*/LAT FSRQs and obeyed by the high redshift BAT blazars. This leads us to favour the hypothesis that its accretion disk is non–standard, having, in its inner regions, a funnel collimating the radiation around the jet axis. An anisotropy factor $\sim$10 is enough to make this object consistent with the jet power – disk luminosity correlation. Consequently, its mass could be smaller (by a similar factor 10).
- For each blazar pointing at us and detected through its beamed non–thermal emission, there should be other $\sim \Gamma^2$ at the same redshift with similar properties, including the mass of the black hole. This puts a lower limit to the density of heavy black holes in the $3 < z < 4$ redshift range.
- Hard X–ray surveys can catch powerful and distant blazars where their high energy SED peaks. This implies that future X–ray missions such as *EXIST* and *NHXM* will be the most effective way to find and study the most extreme radio–loud objects. In the *Fermi*/LAT 0.1–100 GeV energy range these objects, having steep spectra, are less conspicuous and can be missed by *Fermi*. According to the *EXIST* sensitivity in hard X–rays, powerful FSRQs can be easily detected even at redshift 8, if they exist. According to the X–ray luminosity function derived by Ajello et al. (2009), *EXIST* should detect 500–1500 blazars at $z > 4$ and 20–60 at $z > 6$, allowing us to derive the mass function of radio–loud AGN up to very large redshifts.

ACKNOWLEDGMENTS

We thank the anonymous referee for his/her comments. We thank Andrea Merloni and Marco Ajello for discussions. This work was partly financially supported by a 2007 COFIN-MIUR and an ASI I/088/06/0) grants. This research made use of the NASA/IPAC Extragalactic Database (NED) which is operated by the Jet Propulsion Laboratory, Caltech, under contract with NASA, and of the *Swift* public data made available by the HEASARC archive system. We also thank Neil Gehrels and the *Swift* team for quickly approving and performing the requested ToO observations of 1210+330.

REFERENCES

Abdo A.A., Ackermann M., Ajello M., et al., 2009, ApJ, 700, 597
Abramowicz M.A., Czerny B., Lasota J.P. & Szuszkiewicz E., 1988, ApJ, 332, 646
Ajello M., Costamante L., Sambruna R.M., et al., 2009, ApJ, 699, 603 (A09)
Bandara K., Crampton D. & Simard L., 2009, ApJ, 704, 1135
Baes M., Buyle P., Hau G.K.T. & Dejonghe H., 2003, MNRAS, 341, L44
Bassani L., Landi R., Malizia A. et al. 2007, ApJ, 669, L1
Bianchin V., Foschini L., Ghisellini G. et al., 2009, A&A, 496, 423
Böck M., Kadler M. Tosti G., Burnett T., Ohia R., MÜller C. & Wilms J., 2010, proc. of the 2009 *Fermi* Symposium, in press (astro–ph/0912.4192)
Bottacini E., Ajello M., Greiner J. et al., 2010, A&A, 509, A69
Brunthaler A., Falke H., Bower G.C. et al., 2000, A&A, 357, L45
Bryan G.L.& Norman M.L., 1998, ApJ, 495, 80
Cardelli J.A., Clayton G.C. & Mathis J.S., 1989, ApJ, 345, 245
Cusumano G., La Parola V., Segreto A. et al., 2009, A&A, in press (astro–ph/0906.4788)
Donato D., Ghisellini G., Tagliaferri G. & Fossati G., 2001, A&A, 375, 739
Ferrarese L., 2002, ApJ, 578, 90
Foschini L., Ghisellini G., Raiteri C.M. et al., 2006, A&A, 453, 829
Fossati G., Maraschi L., Celotti A., Comastri A. & Ghisellini G., 1998, MNRAS, 299, 433
Frank J., King A. & Raine D.J., 2002, Accretion power in astrophysics, Cambridge (UK) (Cambridge University Press)

Ghisellini G., Celotti A., Fossati G., Maraschi L. & Comastri A., 1998, MNRAS, 301, 451
Ghisellini G., Foschini L., Volonteri M., Ghirlanda G., Haardt F., Burlon D., Tavecchio F., 2009, MNRAS, 399, L24
Ghisellini G., Maraschi L. & Tavecchio F., 2009, MNRAS, 396, L105
Ghisellini G. & Tavecchio F., 2009, 397, 985 MNRAS
Ghisellini G., Tavecchio F. & Ghirlanda G., 2009, MNRAS 399, 2041
Ghisellini G., Tavecchio F., Foschini L., Ghirlanda G., Maraschi L., Celotti A., 2010, MNRAS, in press (astro–ph/0909.0932) (G10)
Gültekin K., Richstone D.O., Gebhardt K. et al., 2009, ApJ, 698, 198
Haiman, Z., 2004, ApJ, 613, 36
Hook I.M., McMahon R.G., Patnaik A.R., Browne I.W.A., Wilkinson P.N., Iwrin M.J. & Hazard C., 1995, MNRAS, 273, L63
Kalberla P.M.W., Burton W.B., Hartmann D., Arnal E.M., Bajaja E., Morras R. & Pöppel W.G.L., 2005, A&A, 440, 775
Li L.–X., Zimmerman E.R., Narayan R. & McClintock J.E., 2005, ApJS, 157, 335
Madau P., 1988, ApJ, 327, 116
Madau P., 1995, ApJ, 441, 18
Maraschi L., Foschini L., Ghisellini G., et al., 2008, MNRAS, 391, 1981
Nandikotkur G., Jahoda K.M., Hartman R.C., Mukherjee R., Sreekumar P., Böttcher M., Sambruna R.M. & Swank J.H., 2007, ApJ, 657, 706
Pareschi G., Tagliaferri G., Attinà P. et al., 2009, Proceedings of the SPIE, Volume 7437, pp. 743704
Pizzella A., Corsini E.M., Dalla Bontà E., Sarzi M., Coccato L. & Bertola F., 2005, ApJ, 631, 785
Poole T.S., Breeveld A.A., Page M.J. et al., 2008, MNRAS, 383, 627
Prochaska J.X., Worseck G., O'Meara J.M., 2009, ApJ, 705, L113
Romani R.W., 2006, AJ, 132, 1959
Roming P.W.A., Kennedy T.E., Mason K.O. et al., 2005, Space Sci. Rev., 120, 95
Sambruna R.M., Tavecchio F., Ghisellini G., Donato D., Holland S.T., Markwardt C.B., Tueller J. & Mushotzky R.F., 2007, ApJ, 669, 884
Sambruna R.M., Markwardt C.B., Mushotzky R.F. et al., 2006, ApJ, 646, 23
Shakura N.I. & Sunyaev R.A., 1973 A&A, 24, 337
Shapiro S.L., 2005, ApJ, 620, 59
Shen Y., Greene J.E., Strauss M.A., Richards G.T. & Schneider D.P., 2008, ApJ, 680, 169
Sheth R.K. & Tormen G., 1999, MNRAS, 308, 119
Schlegel D.J., Finkbeiner D.P., Davis M., 1998, ApJ, 500, 525
Stickel M., Kühr H. & Fried J.W., 1993, A&ASS, 97, 483
Szuszkiewicz E., Malkan M.A. & Abramowicz M.A., 1996, ApJ, 458, 474.
Tanaka T. & Haiman Z., 2009, ApJ, 696, 1798
Tavecchio F., Maraschi L., Ghisellini G., Kataoka J., Foschini L., Sambruna R.M. & Tagliaferri G., 2007, ApJ, 665, 980
Thompson D.J., Bertsch D.L., Dingus B.L et al., 1993, ApJ, 415, L13
Tueller J., Baumgartner W.H., Markwardt C.B., et al. 2009, ApJS, in press (astro–ph/0903.3037)
Volonteri M. & Rees M.J., 2005, ApJ, 633, 624
Volonteri M. & Rees M.J., 2006, ApJ, 650, 669
Yuan W., Fabian A.C., Celotti A. & McMahon R.G., 2005, MNRAS, 358, 432
Yuan W., Fabian A.C., Worsley M.A. & McMahon R.G., 2006, MNRAS, 368, 985
Worsley M.A., Fabian A.C., Turner A.K., Celotti A. & Iwasawa K., 2004a, MNRAS, 350, 207
Worsley M.A., Fabian A.C., Celotti A. & Iwasawa K., 2004b, MNRAS, 350, L67
Watanabe S., Sato R., Takahashi T. et al., 2009, ApJ, 694, 294

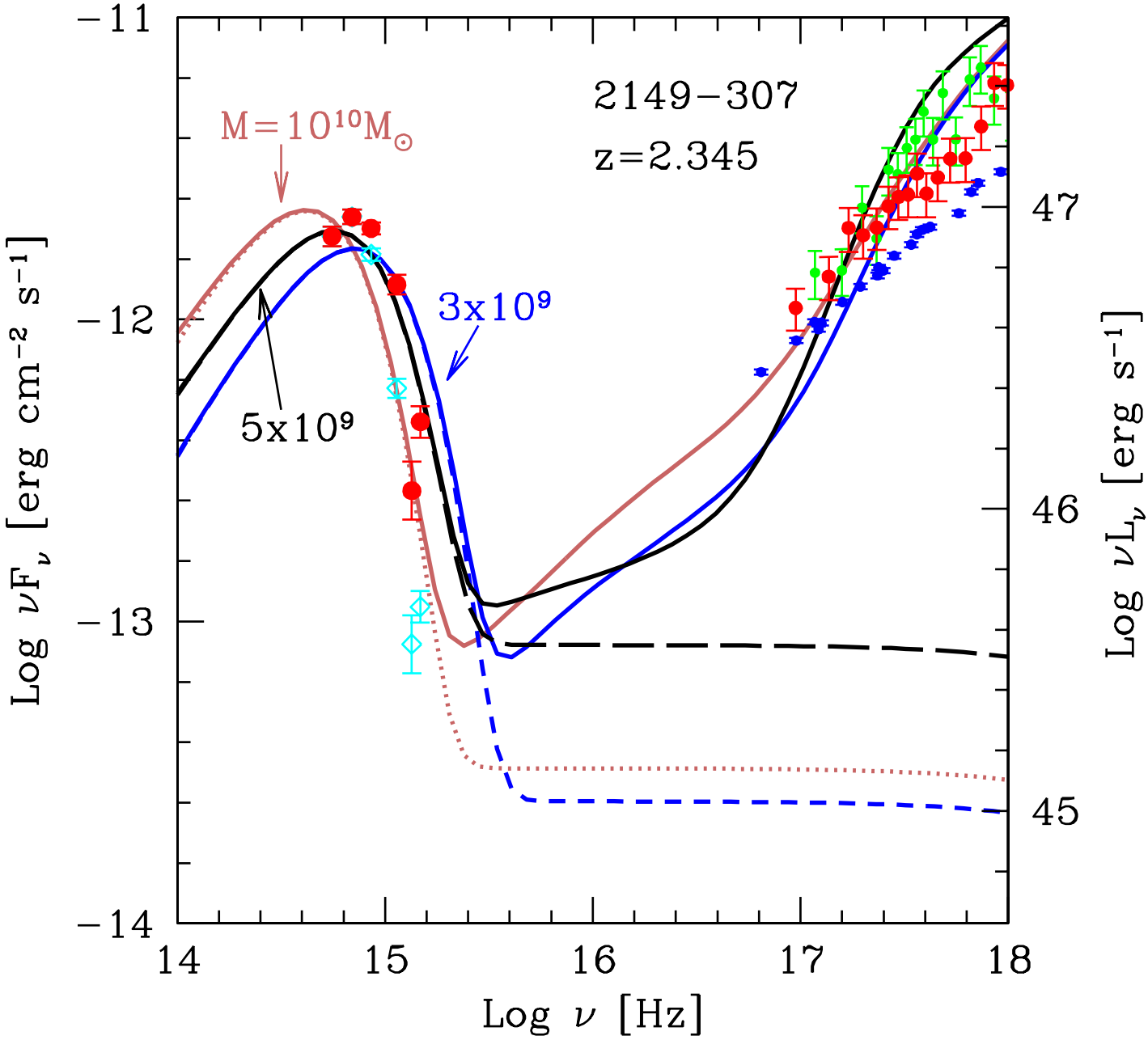
2149−307
z=2.345
M=10¹⁰M⊙
3x10⁹
5x10⁹
Log νF_ν [erg cm⁻² s⁻¹]
Log νL_ν [erg s⁻¹]
Log ν [Hz]
−11
−12
−13
−14
47
46
45
14
15
16
17
18

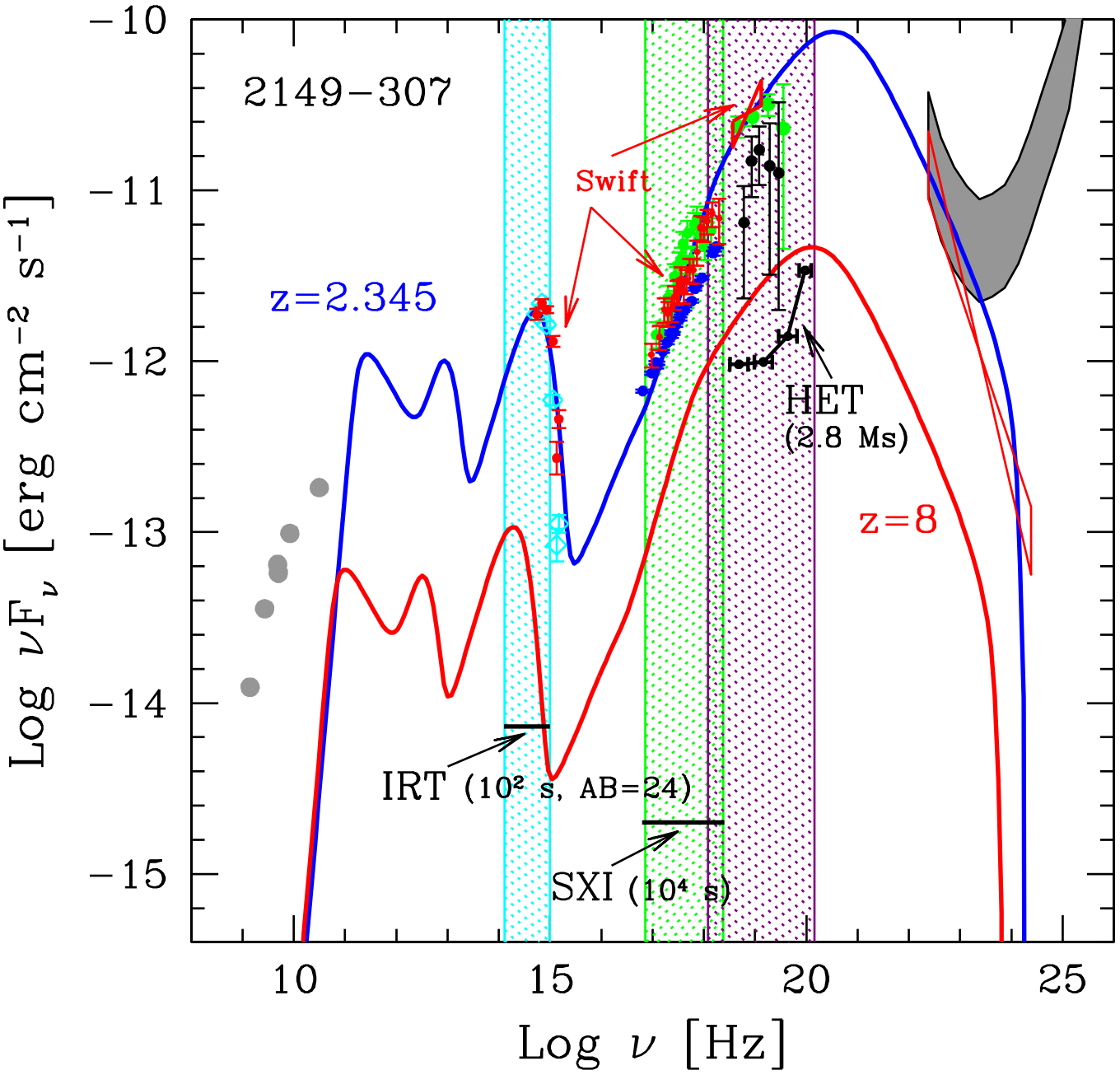
2149−307
z=2.345
z=8
Swift
HET
(2.8 Ms)
IRT (10² s, AB=24)
SXI (10⁴ s)
Log νF_ν [erg cm⁻² s⁻¹]
Log ν [Hz]
−10
−11
−12
−13
−14
−15
10
15
20
25

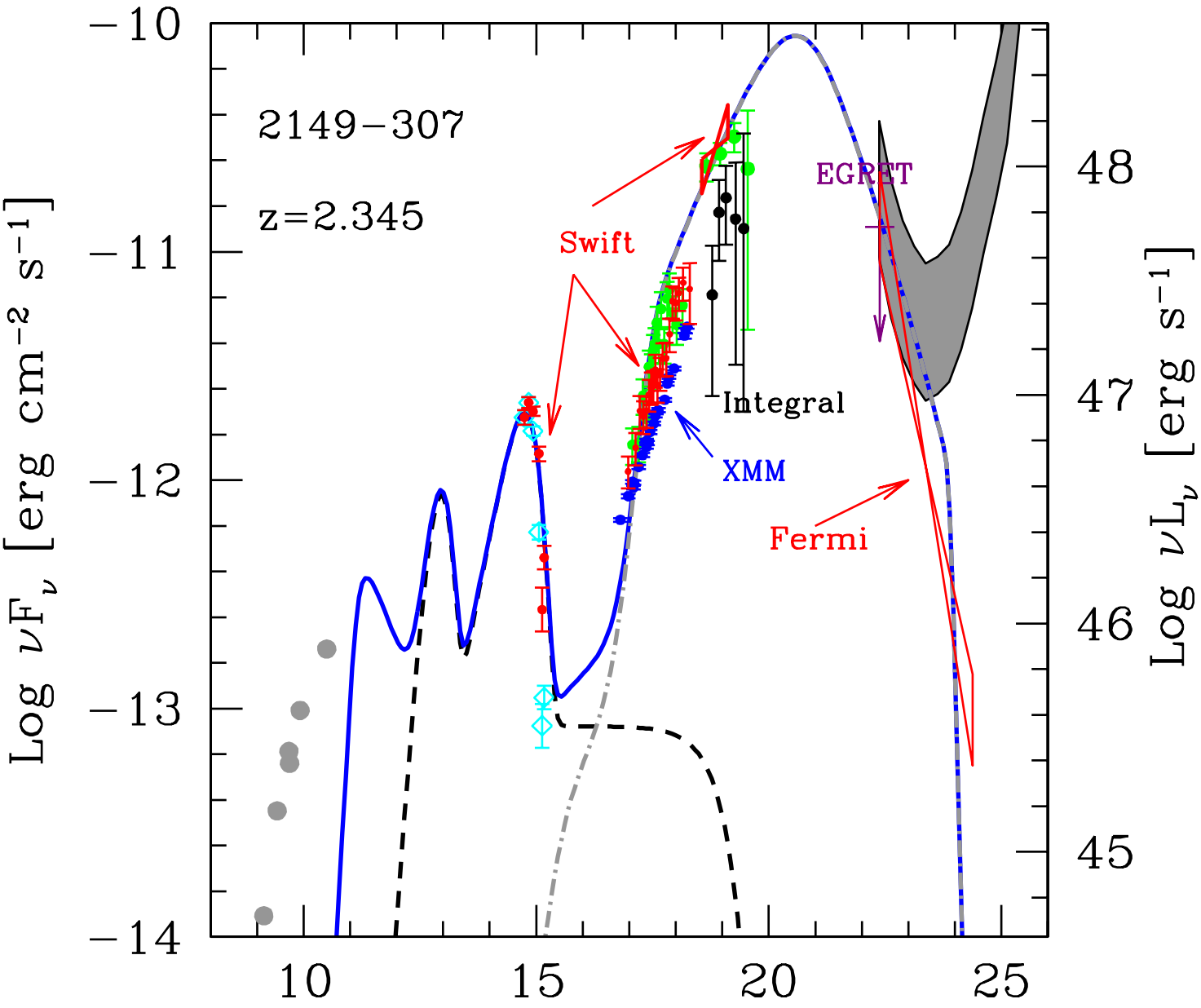
2149−307
z=2.345
Swift
EGRET
Integral
XMM
Fermi
Log νF_ν [erg cm^-2 s^-1]
Log νL_ν [erg s^-1]
−10
−11
−12
−13
−14
48
47
46
45
10
15
20
25